Kovela Granite Complex in southern Finland – mineralogical, geochemical and geochronological study on the origin and P-T evolution

Thair Al-Ani*, Pentti Hölttä, Hugh O'Brien and Kathryn Cutts

Geological Survey of Finland. P.O. Box 96 FI-02151 Espoo, Finland

Abstract

The Kovela Granitoid Complex (KGC) in southern Finland hosts a minor deposit of Th and rare earth elements (REE) associated with crustal melting and magmatic differentiation processes. Such critical element deposits have a high economic and scientific importance. In this paper we deal with the geochemistry, ages and petrogenesis of the KGC rocks.

The KGC comprises three main lithologies: garnet-alkali syeno-monzogranite-granodiorite (Grt-ASMG), monazite-rich pegmatitic tonalite-trondhjemite dikes (Mnz-PTT) and biotite-sillimanite gneiss (Bt-Sil-Gn) xenoliths. Whole-rock geochemistry reveals that Grt-ASMG rocks are peraluminous, high in potassium and silica, and display characteristics of S-type granitoids. Mnz-PTT dikes exhibit significantly higher REE and Th concentrations, with total contents reaching up to 42 000 ppm, with strong negative europium anomalies (Eu/Eu*=0.01–0.05). These geochemical trends, coupled with field observations, suggest that liquid immiscibility played a role in the separation of REE- and Th-enriched tonalite pegmatitic melts from the parent granitic magma.

Monazite grains exhibit complex Th- and LREE-rich zoning, indicative of multiple crystallization and metamorphic events. U-Pb dating of monazite and zircon yields ages ranging from 1.92 Ga to 1.72 Ga, reflecting a prolonged history of magmatic and metamorphic activity. Garnet compositions suggest high crystallization temperature. Peak crystallization conditions, estimated using GB-GPBQ geothermobarometers, indicate granulite-facies conditions at temperature of ~780 °C and pressure of 4–5 kbar. The results suggest that the KGC formed through a combination of crustal melting and liquid immiscibility processes. These findings provide new insights into the enrichment mechanism of Th- and REE-enrichment in the granitic and pegmatitic systems and enhance our understanding of the metallogeny of similar granitoid complexes.

*Corresponding author (email: thair.alani@gtk.fi)

1. Introduction

The geological Survey of Finland (GTK) first identified a uranium-rich province in 1979 at Nummi-Pusula, ~80 km northwest of Helsinki, which was followed by airborne, ground geophysical, and geochemical investigations through 1989 (Seppänen 1981; Räisänen 1989). The locally high Th values in the neighbouring Kovela region (Fig. 1) prompted further investigations under GTK's high tech metals project (Lahti & Kärkkäinen 2009).

Petrographic studies detailed the extant mineral assemblages, the presence of REE mineralization and the common partial alteration of biotite and plagioclase to chlorite and sericite, respectively. The monazite-bearing dikes show enrichments of Ce (180–1700 ppm), La (790–8100 ppm), Nd (740–7000 ppm), Pr (210–2000 ppm), Sm (120–1200 ppm) and Gd (90–620 ppm). Thorium contents vary between 1100 to 10000 ppm and uranium (U) contents are between 5 and 320 ppm.

The dominant rock type in the KGC is a microcline granite, which occurs over the entire region, while garnet-bearing gneiss, as well as marginal pegmatite bodies occur along the outer contact of the complex (Fig. 2). The high level of radioactivity in the KGC mainly results from the presence of Th-rich Mnz-PTT dikes. These dikes are most predominant in the central zone of the complex and also present in lesser amounts in the surrounding country-rocks. Most of the Mnz-PTT dikes run roughly in a NW-SE direction and are named according to their locations: S-dikes in the southern part and N-dikes in northern part of the complex (Fig. 2). The dikes are usually 5–10 m wide and 60–70 m long with a gentle dip to the west. The S dikes are more highly enriched in Th thorium than the N dikes and are composed mainly of perthitic feldspar, quartz, plagioclase, biotite, garnet, sillimanite, and cordierite, with accessory monazite, zircon, apatite, ilmenite, and chlorite.

The (Mnz-PTT) dikes are characterized by high REE and Th contents, ranging between 0.6 to 4.3 wt.% and 0.01 to 1.3 wt.%, respectively, with U contents between 3 to 320 ppm (Sarapää et al. 2015). The KGC underwent granulite facies metamorphism, with peak pressure-temperature (P–T) conditions estimated at 700 to 820 °C and 3 to 6 kbar (Al-Ani et al. 2019). In this study, we present new geochemical, mineral chemistry and isotopic data for the main lithologies of the KGC, including the monazite-rich pegmatitic granite dikes.

2. Geological setting

The Svecofennian orogen in Fennoscandia was created by a long-lived orogeny characterized by low-pressure, high-temperature (LP-HT) metamorphism (Hölttä et al. 2020; Salminen et al. 2022). The orogen has been divided into Western Finland (WFS) and Southern Finland Subprovinces (SFS) of the Paleoproterozoic Svecofennian domain (Nironen 2017 & Fig. 1). The boundary between the WFS and SFS is both tectonic and metamorphic where the migmatites in the southern part of the WFS changed into andalusite schists and sillimanite-biotite-muscovite gneisses in the SFS along a roughly E-W strike shear zone (Hölttä et al. 2020). The Svecofennian Orogen was formed by accretion of island arcs and ophiolites against the Archaean craton between c. 1.92 and 1.77 Ga (Gaál & Gorbatchev 1987; Nironen 1997; Lahtinen et al. 2023; Heilimo et al. 2023). Collisional tectonics and possible magmatic underplating thickened the crust to its maximum thickness of 65 km in central Finland and < 50 km in southern Finland (Korja & Heikkinen 2005). The continental collision occurred simultaneously with high–T and low–P metamorphism and crustal melting in southern Finland and south-central Sweden, including I- and S-type granitic rock magmatism (Andersson & Öhlander 2004; Kurhila et al. 2005).

The Kovela Granite Complex (KGC) is located in the western part of the Uusimaa Belt (Fig. 1). The main lithologies of the Uusimaa Belt are 1.90–1.88 Ga felsic to mafic metavolcanic rocks (Lahtinen 1996; Skyttä et al. 2005), metasedimentary rocks,
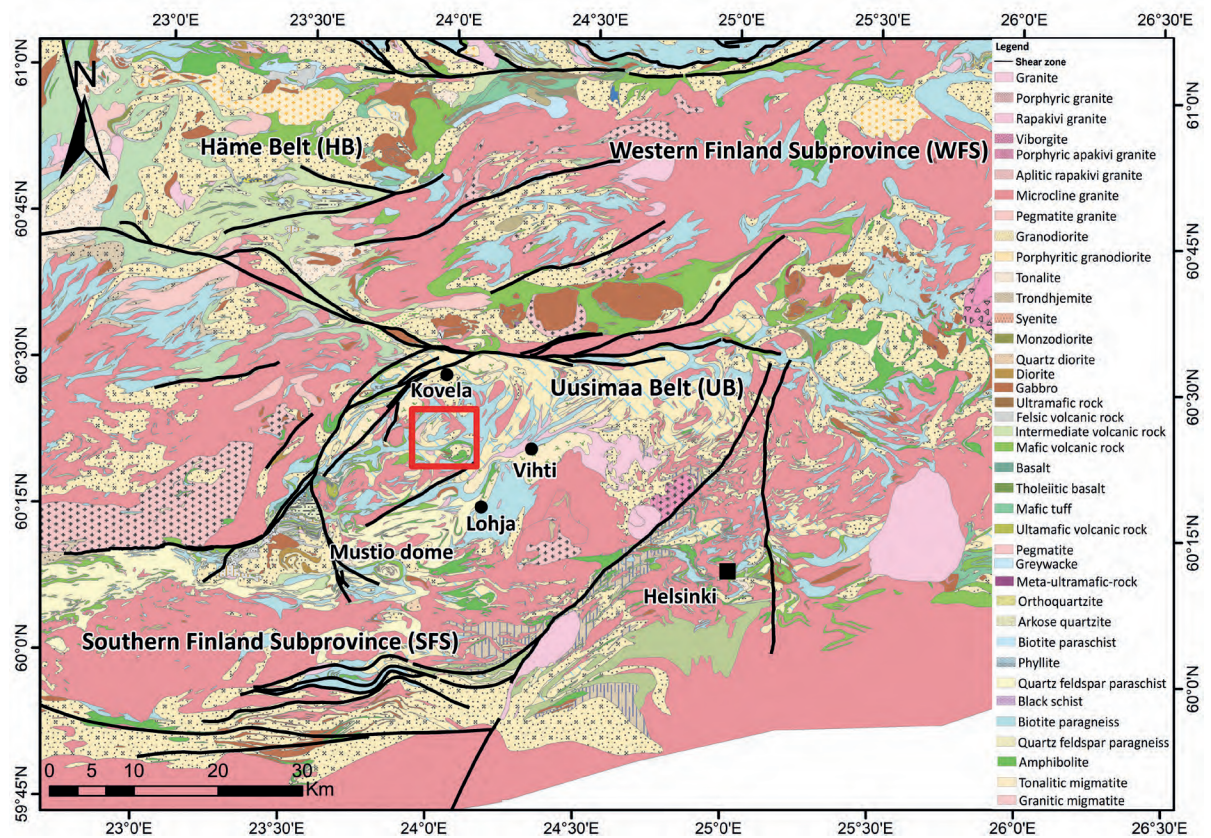
Figure 1. Geological map of South Finland, modified from Nironen (2017) and based on digital bedrock data from geological survey of Finland GTK. The red rectangle indicates the study area. The bedrock map is constructed using digital map information from GTK: https://gtkdata.gtk.fi/Kalliopera/index.html; © Geological Survey of Finland (2016, GTK Basic license version 1.1), Bedrock of Finland 1:200 000 (2023–2024), CC-BY-4.0

early Svecofennian 1.90–1.88 Ga gabbroic to tonalitic rocks (Ehlers et al. 2004; Väisänen et al. 2002), and late Svecofennian 1.85–1.80 Ga granitic rocks derived from partial melting of the crust (Huhma et al. 2011, 2012; Suominen 1991; Jurvanen et al. 2005, Kurhila et al. 2005).

There are several previous studies on the deformation history and metamorphic conditions of the Uusimaa Belt, surrounding the Kovela Granite Complex (KGC). According to Skyttä & Mänttäri (2008), the deformation patterns and voluminous granitic magmatism of late Svecofennian granites and pegmatites in Uusimaa Belt, occurred at ~ 1.85–1.80 Ga. Mouri et al. (2005) estimated that the peak metamorphic conditions of West Uusimaa (4–5 kbar and

750–800°C), occurred between 1832±2 Ma and 1816±2 Ma. Schreurs & Westra (1986) conducted the first pressure-temperature (P–T) studies in the Western Uusimaa region. Their research estimated peak metamorphic conditions in the area to be approximately 750–800 C and around 4–5 kbar, occurring under water-undersaturated conditions. Based on Al-Ani et al. (2019), the peak metamorphic conditions of the KGC have been estimated at 760–770 °C and 5–6 kbar with U-Pb monazite dating yielding a wide range of ages between 1796 ± 16 Ma and 1912 ± 28 Ma. According to Pajunen et al. (2008), although the Svecofennian orogen in Fennoscandia was a continuous process, several local tectono-thermal discordances led to differences in stabilization times
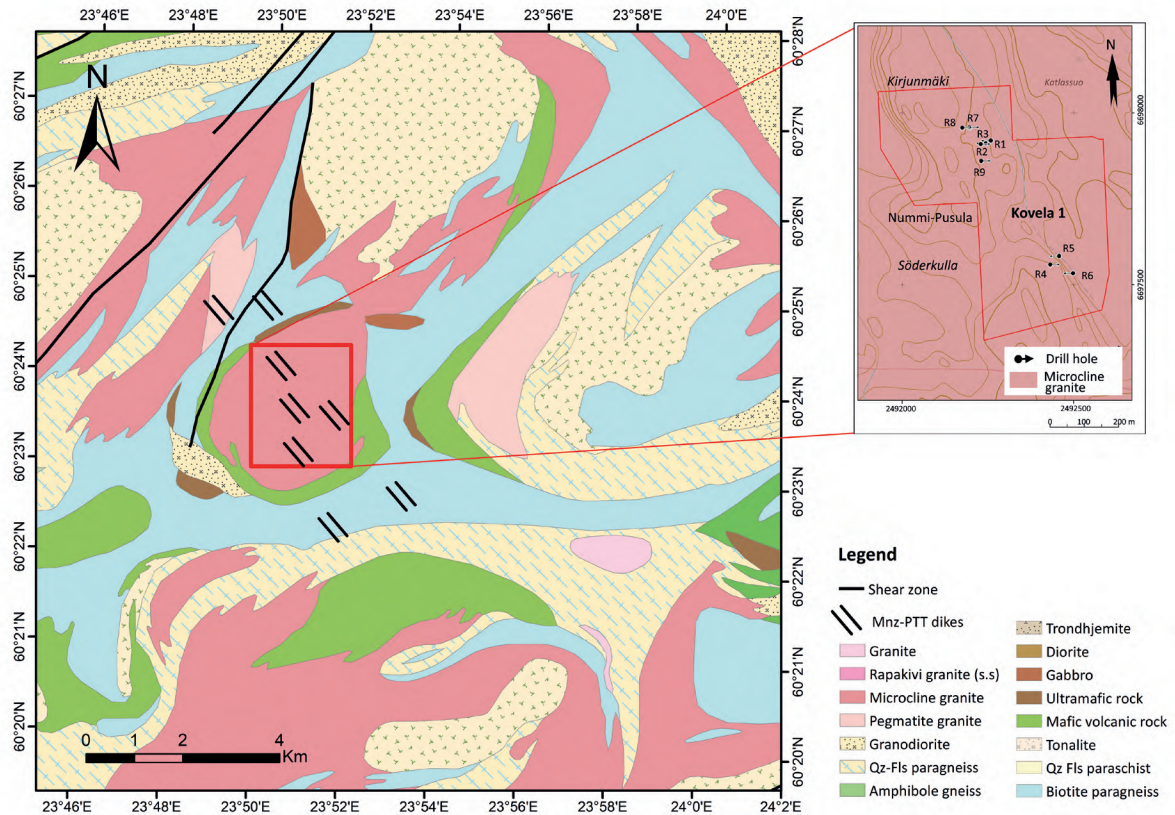
Figure 2. Geological map of the Kovela Granitoid Complex KGC, modified from Digital Bedrock Map of Finland (as referred to the previous Fig. 1). Grt-ASMG=garnet-alkali syeno-monzogranite-granodiorite; Mnz-PTT monazite-rich pegmatitic tonalite-trondhjemite dikes.

across tectonic units. For instance, while some units like the tectonic migmatite belt stabilized earlier, other such as the Southern Finland Granitoid Zone remained thermally active longer. Some evidence has also been presented for an early metamorphic event around 1.88 Ga in the rocks of western Uusimaa Belt. These variations resulted in distinct post-tectonic evolution, with areas affected by late high-temperature metamorphism entering the brittle deformation stage up to 70 million years later than earlier stabilized regions.

The origin of the high-temperature, medium-pressure granulite metamorphism in the Uusimaa Belt, with an age of 1.83–1.81 Ga (Mouri et al. 2005; Skyttä & Mänttäri 2008), may have been caused by a temperature increase due to crustal thickening (Korsman et al. 1999; Kukkonen &

Lauri 2009), or due to the presence of a hot mafic layer at a depth of 30 to 40 km and CO_2 flushing (Schreurs & Westra 1986).

The Kovela Granite Complex is characterized by a dome-like structure consisting of several generations of magma emplacement with heterogenous, partly pegmatitic granitoids and garnet-monzogranite bodies occurring in the centre of the pluton and mafic volcanic and ultramafic rocks occurring on the margins. A migmatitic paragneiss containing biotite ± sillimanite, as well as marginal pegmatitic tonalite-trondhjemite bodies are found along the outer contact of the complex (Fig. 2). Small intrusive bodies of amphibolite and gabbro are also associated within the wall rocks of the KGC. Th-rich Mnz-PTT dikes are abundant in the central zone and are also present, although less

common, in the surrounding wall rocks (samples R3_0.5, R3_4.40 and R8_18.50; Fig. 3d–f). Most of these dikes strike roughly NW-SE (Fig. 2). They are relatively small, but dimensions can vary from a few meters to hundreds of meters in the longest dimension and from 5 to 10 meters in width.

3. Materials and methods

Geological field work, geophysical measurements and drilling were carried out by GTK during 2009–2012. Petrographic and mineralogical studies of 45 polished thin sections were carried out using a combination of optical microscopy and a scanning electron microscope (SEM). The mineral compositions of garnet, biotite, plagioclase, sillimanite, cordierite and monazite grains were analysed with a CAMECA SX100 electron microprobe analyser (EMPA) at GTK. X-ray maps of Y, Ce, La, U and Th were acquired in stage scan mode at 20 kV accelerating voltage, 100nA beam current, and 100–200 ms dwell time. Quantitative analyses were performed under 20 kV accelerating voltage 6–60 nA beam current, and 1–10 μm beam diameter, with lower currents and larger diameters applied to beam sensitive phases. Analytical precision, determined from repeated analyses of standards, was typically ≤1–2% relative for major-element oxides (>10 wt.%), 3–5% for minor-element oxides (1–10 wt.%), and <10 for trace elements oxides. The coefficient of variation (CV) was consistently below 5 % for repeated measurements. Values below the detection limits are reported as "<LOD" in the tables. The geothermobarometry estimate results of selected samples are presented in Electronic Appendix 6.

Major-element oxide contents were measured by X-ray fluorescence (XRF) spectrometry and trace elements concentration were determined using inductively coupled plasma-mass spectrometer (ICP–MS) at Eurofins Labtium Ltd, Finland. Analytical methods followed Labtium protocols 175x (XRF) and 307M (ICP-MS). Samples preparation included drying at 70 °C, fine crushing to >2 mm using Cr-steel jaws, splitting with a riffle splitter, and grinding in a harder carbon steel vessel. Accuracy and precision of the analyses were assessed using references materials and internal quality control samples. For XRF, duplicate sample analysis and repeated measurements of standards (QC1 & QC2) showed accuracy within ±2.2 % and precision (standard deviation) typically below 0.08 wt.% for major oxides such as Fe_2O_3 and Al_2O_3. For ICP-MS, QCSDC-1 standard was used with measured values deviating less than 5% from recommended compositions for most trace elements. These analytical constraints are consistent with those reported by Karvinen et al. (2025) and Rasilainen et al. (2007), who provide detailed descriptions of Labtium's geochemical protocols and quality control procedure. The open-source software Geochemical Data Toolkit in R (GCDkit-version 4.1; Janoušek et al. 2006) has been used for whole-rock XRF data processing and classification diagrams in this study. The whole-rock geochemistry of 140 samples and more detailed information about accuracy and precision can be found in Electronic Appendix 7.

Prior to the LA-ICP-MS analyses, monazite and zircon grains were identified and imaged in eight thin-sections using a JEOL JSM5900 LV scanning electron microscope (SEM) equipped with an energy dispersive x-ray spectrometer (EDS) and with INCA software for phase detection and classification to characterize the grain size, shape, and mineral composition. The monazite and zircon grains were dated with LA-ICP-MS at the Geological Survey of Finland, Espoo. Ablations were carried out in a HelExII ablation cell under a helium atmosphere (flow of 0.4 and 0.1 l/min) mixed with argon (flow of 0.93-0.95 l/min) before entering the ICP-MS (Müller et al. 2009). Plotting of the U-Pb isotopic data and age calculations were performed using the program Isoplot v.3 (Ludwig 2003). Other analytical conditions and information on the standards are included in Electronic Appendix 8.

4. Results

4.1. Petrography

Two main rock types are distinguished in the studied drill cores of the KGC: heterogenous, partly pegmatitic and garnet-bearing granitoids —referred to in the introduction as microcline granites— whose composition varies from alkali-feldspar granite to syenogranite, monzogranite and granodiorite (Fig. 3a, b), abbreviated here as Grt-ASMG, and Th-rich monazite pegmatitic tonalite-trondhjemite dikes (Mnz-PTT). Biotite-sillimanite gneiss (Bt-Sil-Gn) inclusions were also found in some drill cores. Near the northwestern drilling sites, the granite has a few inclusions of garnet-rich, foliated felsic gneisses (Fig. 3c).

4.1.1. Garnet-alkali syeno-monzogranite-granodiorite (Grt-ASMG)

The Grt-ASMG unit shows either a weak or no foliation. Garnet is often present, comprising locally up to 5 vol.% of the rock and is found as megacrysts (≤3 cm in diameter) surrounded by coarse grained K-feldspar, plagioclase and quartz producing a 'red-eye socket' texture (Fig. 3a). K-feldspar crystals are mostly anhedral to subhedral, up to 1 by 2 cm in diameter, and are found with garnet, plagioclase, quartz, sillimanite and cordierite. We selected Grt-ASMG samples R1_27.70, R2_17.30, R8_40.7 and R9_10.1 from the drill cores for the detailed petrographic study of this lithological unit.

Under plane-polarized light, the garnet is red-coloured, subhedral millimetre-sized (1 mm-up to 2 cm in diameter) and contain irregular cracks (Fig. 4a-d). Inclusions of quartz, plagioclase, chlorite, sillimanite, zircon, and monazite are widely distributed in the garnet megacysts (Electronic Appendix 9: Fig. S1a-d). Microstructures in the garnet megacysts record both brittle and ductile deformation. Fractures in garnets often show offsets on the order of a few hundred micrometres, and typically extend from one side of the garnet to the other. Most of these fractures are hairline in width,

filled by chlorite and muscovite. However, not all fractured segments of every garnet crystal have been extended or filled with matrix minerals (quartz and feldspar) or with retrograde minerals (biotite and chlorite) (Electronic Appendix 9: Fig. S1a-d). This suggests that garnet fracturing in the samples occurred at shallow crustal depths as these anisotropic rocks responded to horizontal extension during uplift and cooling of the metamorphic terrane (Hawemann et al. 2019a, b; Prior 1993; Prior et al. 2000, 2002).

4.1.2. Monazite-rich pegmatitic tonalite-trondhjemite dikes (Mnz-PTT)

All the Mnz-PTT dikes are medium-to coarse-grained, equigranular to porphyritic rocks (Fig. 3d), plagioclase being the main phenocryst phase and more abundant than K-feldspar. The rock consists of variable abundances of plagioclase (46.5–81.7 %), quartz (6.5–38.8 %), K-feldspar (4.5–28.5 %), quartz (6.5–39.0 %), cordierite (1.2–4.7 %), and opaque Fe-Ti oxide (0.3–1.2). They contain minor to accessory (<1%) amounts of biotite, sillimanite, garnet, apatite, and monazite (Fig. 4f). Although monazite is only an accessory mineral, it is visible to the naked eye in the most Mnz-PTT samples. Monazite occurs mainly as elongated prismatic crystals (up to 2 mm in diameter), platy tabular and euhedral to subhedral grains (Fig. 4f). It is the main host for REE, Th and U in the KGC lithologies. Thorite appears as inclusions within monazite and zircon (Fig. 4f). Most Mnz-PTT samples are generally fresh, with only some samples showing minor alteration of plagioclase grains to sericite and some biotite to secondary chlorite.

4.1.3. Biotite-sillimanite gneiss (Bt-Sil-Gn)

Bt-Sil-Gn rock samples are grey to dark grey, grain size ranges from fine to medium. This rock type is rich in mafic minerals, up to 30–45 %, comprising varying proportions of biotite, chlorite, and garnet, along with 10–20 % quartz and 25–30 %
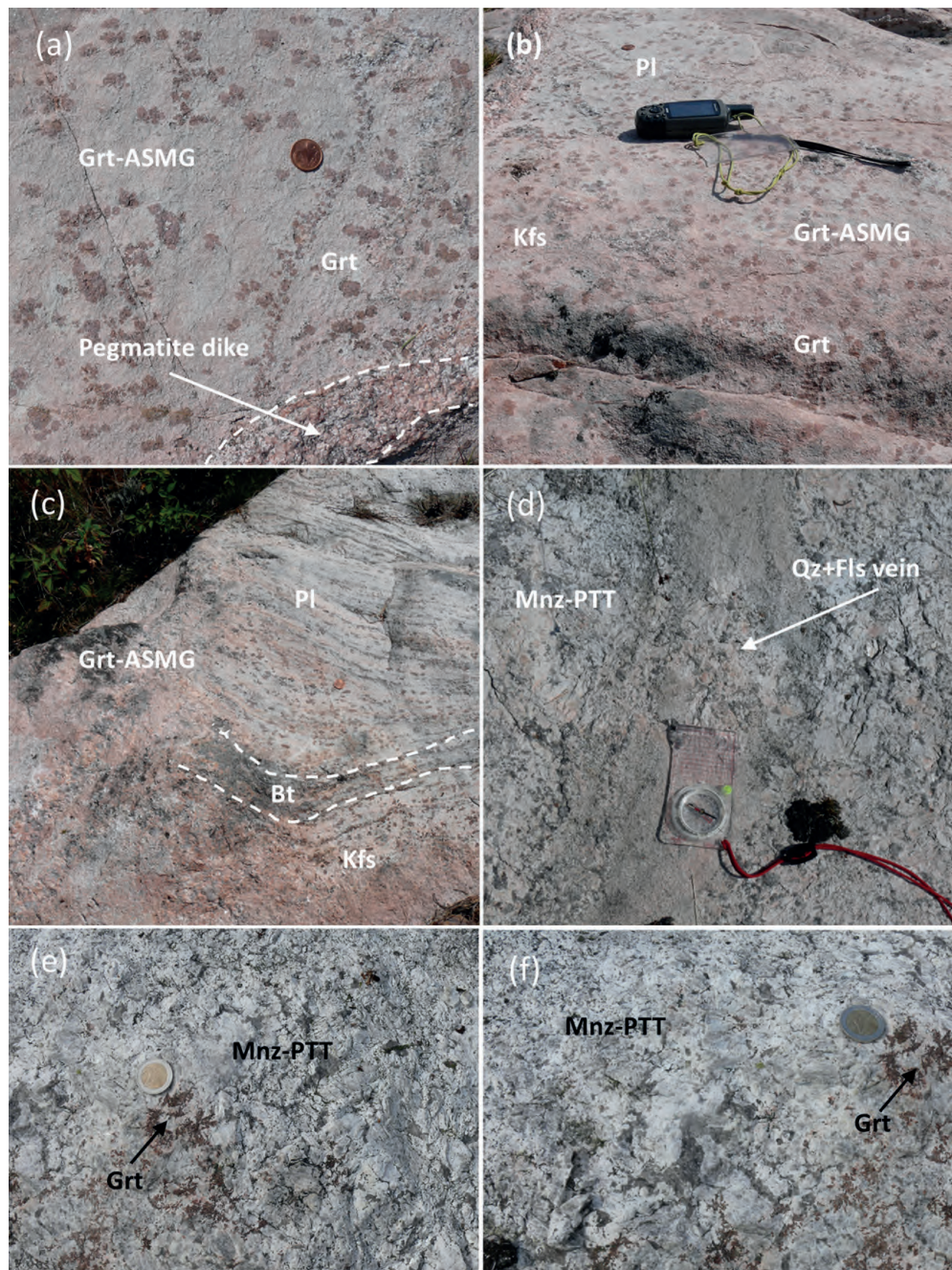
Figure 3. Outcrop-scale features of the KGC and associated rocks, 2€ (diameter: 25.75 mm), 5 cent (diameter: 21.25 mm) coins and compass (diameter: 50–100 mm) used for scale. (a, b) Weakly foliated garnet-alkaline granite-granodiorite (Grt-ASMG) with pinkish to brownish garnet crystals (megacrysts), up to 2 cm in size, that often appear on the outcrop surface in comparison to matrix. The outcrop also shows pegmatitic dikes of 2 to 5 m in length and 0.05 to 0.5 m in width with sharp contacts to Grt-ASMG (only shown in a). (c) Foliated garnet-rich felsic gneiss monzogranite. Garnets show red-eye socket texture with no replacement by secondary minerals. The dashed lines mark rock foliations. (d-f) Grey, coarse-grained Th-rich monazite-bearing pegmatitic granite dikes (Mnz-PTT) with tonalite to trondhjemite compositions. The outcrop also displays quartzo-feldspathic veins (only shown in d).

plagioclase. This rock type also contains about 10 % Al silicates (andalusite, kyanite and most commonly sillimanite) and Fe–Mg–Al silicate (cordierite) in many places. Garnet occurs as inclusion-rich megacrysts (up to 0.5 cm in diameter) with irregular grain boundaries (Fig. 4c, d). The inclusions are evenly distributed in the garnet and comprise chlorite, quartz, zircon and sillimanite. Garnet is surrounded by sillimanite and biotite along its rims and occurs preferentially in layers modally rich in sillimanite and biotite. Sillimanite occurs as foliation parallel matrix crystals and porphyroblasts up to 2 mm in length showing fibrofilic habit (Fig. 4d, e), and as fine to coarse grains dominantly as fibrolite aggregates formed by needle-like and blade-shaped crystals (Fig. 4e). Biotite forms euhedral to subhedral discrete flakes, measuring up to 2 mm in length or aggregates intimately associated with muscovite, sillimanite, chlorite, and/or Fe-Ti oxides (Fig. 4a–d). Biotite commonly contains inclusions of zircon, monazite, and quartz. Biotite flakes are frequently altered to chlorite, either completely or partially along {001} cleavages. Muscovite flakes typically occur as overgrowths on biotite representing replacement products of biotite, and also occur as fracture and cavity fillings in garnets (Electronic Appendix 9: Fig. S1 c, d).

4.2. Mineral compositions

Mineral compositions and structural formulas of KGC lithological phases are listed in Electronic Appendices 1 to 5.

4.2.1. Garnet

Microprobe analyses of some garnet grains from the KGC rocks show a continuous chemical zoning, where FeO and MnO are slightly increasing and MgO and CaO slightly decreasing from core to rim (Electronic Appendix 9: Fig. S2c, d). These element patterns are consistent with weak zoning developed under decreasing temperature and pressure conditions (Spear 1993; Kohn 2003).

The results of major element analysis of the garnet grains from KGC lithologies are listed in Electronic Appendix 1. Garnet megacrysts are dominantly almandine (XFe = 0.76–0.83), lesser amounts of pyrope (XMg = 0.08–0.16), spessartine (XMn = 0.04–0.10) and grossular (XCa = 0.03–0.05) (Electronic Appendix 9: Fig. S1 & S2). The XMg values range from 0.17–0.09 from the core to rim. Most microprobe analyses show that garnet is weakly zoned, with Fe- Mn-poor cores and Fe- and Mn-rich rims (Electronic Appendix 9: Fig. S2a, b). The flat major element profiles of garnets in most of the studied samples are typical for grains that have been completely homogenized under peak metamorphic conditions (e.g., Tuccillo et al. 1990). However, a few of the analyzed garnet megacrysts exhibit increasing Fe and Mn and decreasing Mg and Ca toward the rim (Fe, core-rim: 2.33–2.55 a.p.f.u; Mn: 0.13–0.29; Mg, 0.50–0.23 a.p.f.u; Ca, 0.15–0.03 a.p.f.u), suggesting that these garnet grains grew under low-pressure conditions.

The chemical analyses of garnet were plotted in a ternary diagram (Mange & Morton 2007), with XMg (pyrope), XCa (Grossular) and XFe+Mn (almandite+spessartine) (Fig. 5a). The KGC garnet data plot within the type B fields, mainly in the sub-field Bi. Most of the garnets are almandine (mean of 50 analyses = $Alm_{0.8}Prp_{0.11}Grs_{0.03}Sps_{0.06}$). A global study of garnet-bearing magmatic rocks by Kemp et al. (2007) proved that almandine in S-type granites and metapelites has low CaO (< 4 wt.%) and variable MnO contents (Fig. 5b), and is usually associated with quartz, biotite, K-feldspar, plagioclase, and cordierite. Consistent with this, the KGC garnets from Grt-ASMG and Th-rich Mnz-PTT show strong affinity to S-type magmatic garnets, while garnets from Bt-Sil-Gn mostly plot in the metapelitic garnet field.

4.2.3. Biotite

The structural formulae of biotite were calculated based on twenty-two oxygens, $(OH)_2$ excluded. The total iron is represented as Fe^{+2}. The chemical
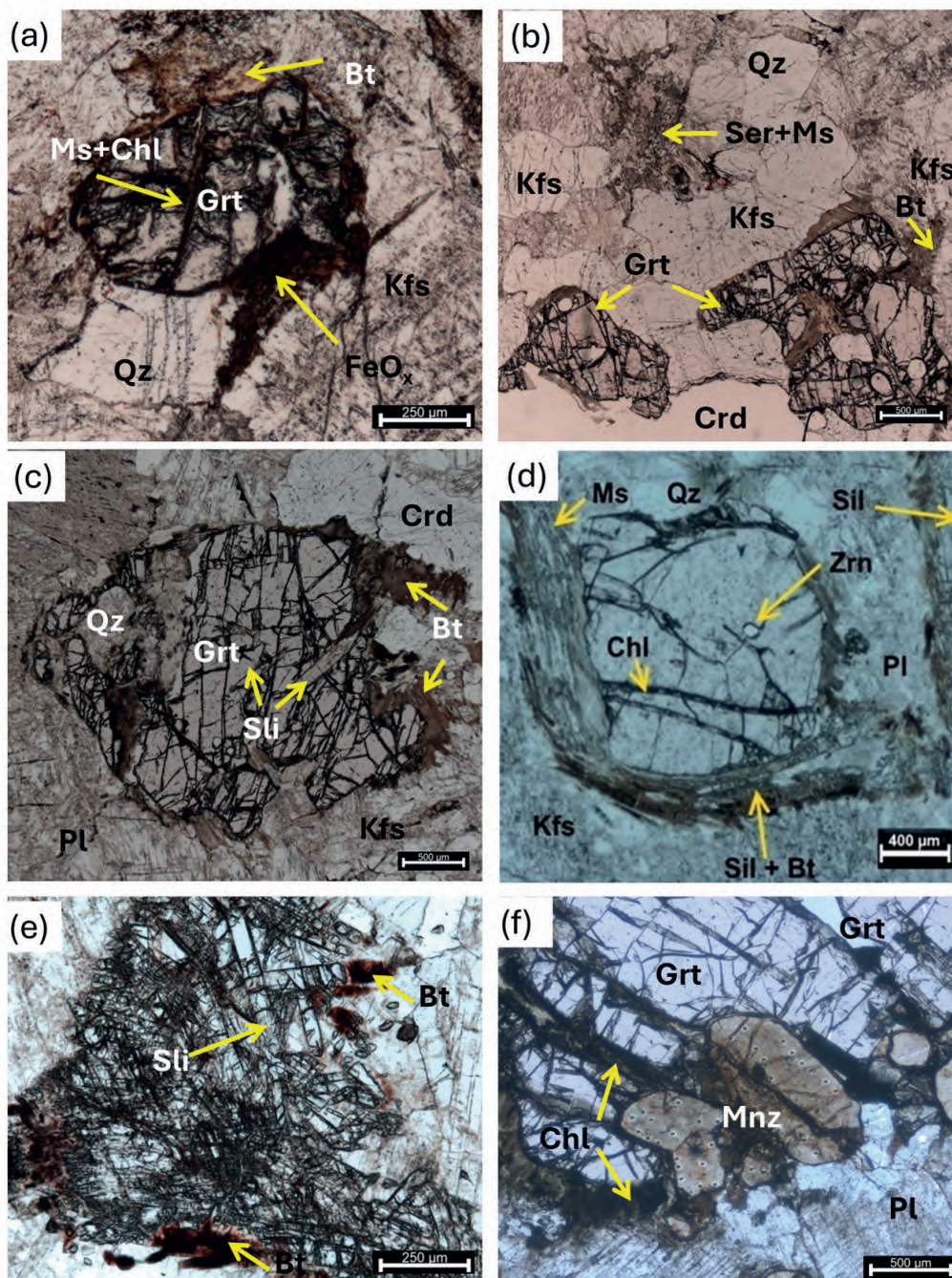
Figure 4. Thin section-scale petrographic features of the KGC rocks (a–e in plane-polarized light, f in cross-polarized light). (a) Representative peak mineral assemblages in the garnet-alkaline syeno-monzogranite-granodiorite (Grt-ASMG) rock sample R2_17.30, consisting of garnet, quartz, biotite, and feldspar. (b) Garnet aggregates in biotite-muscovite-quartz matrix in Grt-ASMG sample R1_27.70. (c) Fracturing and plastic deformation of garnet megacrysts in biotite-sillimanite gneiss Bt-Sil-Gn sample R1_29.75. (d) Garnet megacrysts next to sillimanite and biotite in Bt-Sil-Gn sample R9_23.20. (e) Sillimanite occurs as high relief, needle-like, bladed shapes in Bt-Sil-Gn sample R1_29.75, (f) Grt-ASMG associated with garnet megacrysts from monazite-bearing pegmatitic tonalite–trondhjemite (Mnz-PTT) sample R3_4.40, also showing fractures filled by chlorite.
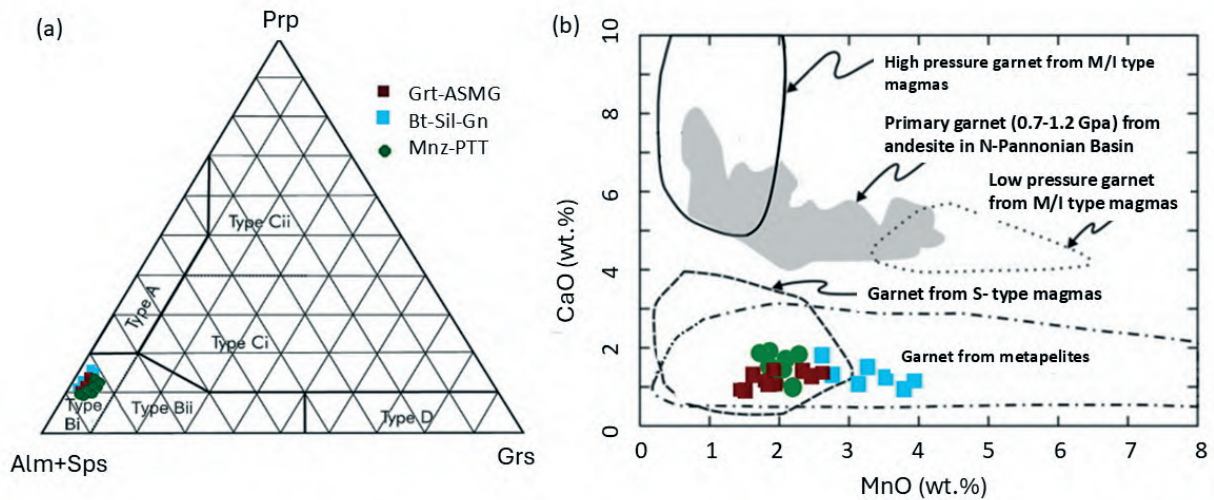
Figure 5. (a) Ternary discrimination diagram after Mange and Morton (2007) showing that all analyses garnets from the KGC plot within field Bi, indicating an amphibolite-facies metasedimentary source. Field A= high-grade granulite-facies metasedimentary rocks, charnockites and intermediate to felsic igneous rocks; Bi= amphibolite-facies metasedimentary rocks; Bii=intermediate to felsic igneous rocks; Ci= high-grade mafic rocks; Cii= ultramafic with high Mg content (e.g. pyroxenites and peridotites); D=metasomatic rocks, very low-grade metamafic rocks and ultrahigh-temperature metamorphosed calc-silicate granulite. (b) CaO versus MnO diagram after Harangi et al. (2001), showing a distinct compositional trend among KGC garnets. The Mn-rich and Ca-poor compositions are consistent with garnet growth in metasedimentary environment under amphibolite facies conditions.

composition of biotites indicates pronounced variations in the Al_{Tot}, Mg, Ti contents and $Fe^{+2}/(Fe^{+2}+Mg)$ values (Electronic Appendix 2). Biotites from KGC samples mostly plot in the field of biotite-siderophyllite, showing generally high $Fe^{+2}/(Fe^{+2}+Mg)$ values (0.57–0.73) and high Al_{Tot} contents (3.42–4.10) apfu (Fig. 6a).

Nachit et al. (2005) proposed the ternary diagram $10*TiO_2 – (FeO + MnO) – MgO$ to use biotite chemical composition as a quantitative tool for distinguishing among biotites that are primary magmatic, re-equilibrated, or secondary, formed by or within hydrothermal fluids (Fig. 6b). The investigated biotite from Grt-ASMG and Mnz-PTT samples predominantly plot in the field of primary biotite or re-equilibrated primary biotites, while all analyzed biotites from Bt-Sil-Gn samples scatter within the field of secondary biotite. On a microscopic scale, biotite and chlorite are common features of retrograde alteration of high-grade metamorphic rocks in the KGC. Regarding the chemical composition of secondary biotite,

chloritization causes biotite to become more iron-rich and Ti-poor compared with primary magmatic biotite.

4.2.4. Plagioclase and cordierite

Representative microprobe analyses of plagioclase grains are given in Electronic Appendix 3. Plagioclase either forms inclusions in garnet (smaller grains 0.05 mm) or occurs as matrix grains (coarser grains) in contact with garnet and biotite reaching up to 10 mm in diameter. Most of analyzed rock samples show plagioclase crystals that have broadly similar compositions ranging from An 65.0–31.0 mol.%, Ab 68.3–84.5 mol.% and Or 0.30–2.1 mol.%. However, most are zoned from calcium–rich in the center to more sodium–rich rims having core compositions between $An_{21–31}$ and $Ab_{68–79}$, and rim compositions ranging from $An_{16–27}$ and $Ab_{72–83}$. The analysed cordierite grains from two samples, R2_17.30 and R8 _18.50 are predominantly magnesian (Fe/(Fe + Mg)) <0.5),
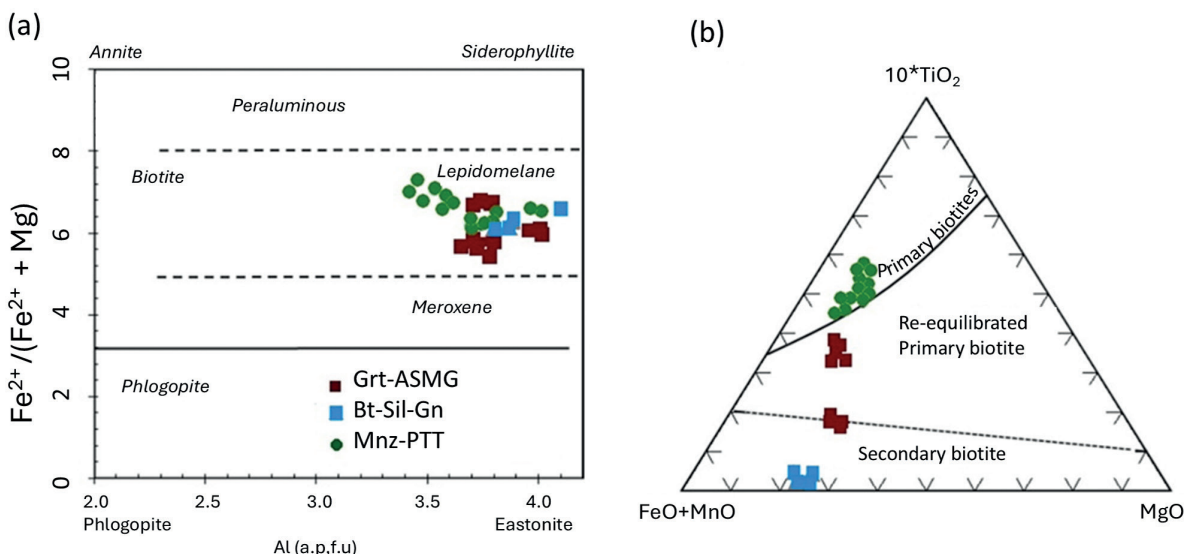
Figure 6. The investigated biotite from garnet-alkaline syeno-monzogranite-granodiorite (Grt-ASMG), monazite-bearing pegmatitic tonalite–trondhjemite Mnz-PTT, and biotite-sillimanite gneiss (Bt-Sil-Gn) samples (a) Compositional plot of biotite in the phlogopite–annite–siderophyllite–eastonite system. The subdivision of tetrahedral micas (heavy line; after Deer et al. 1992) and the biotite classification (dashed line; after Tröger et al. 1979). (b) Biotite compositions in the $10*TiO$ – $(FeO + MnO)$ – MgO ternary diagram (wt.%), with limits of the domains for magmatic, re-equilibrated and secondary biotite after Nachit et al. (2005).

ranging from 0.2 to 0.45 (Electronic Appendix 4). This compositional range could be attributed to either a metamorphic or igneous origin, based on the criteria outlined by Schreyer (1985).
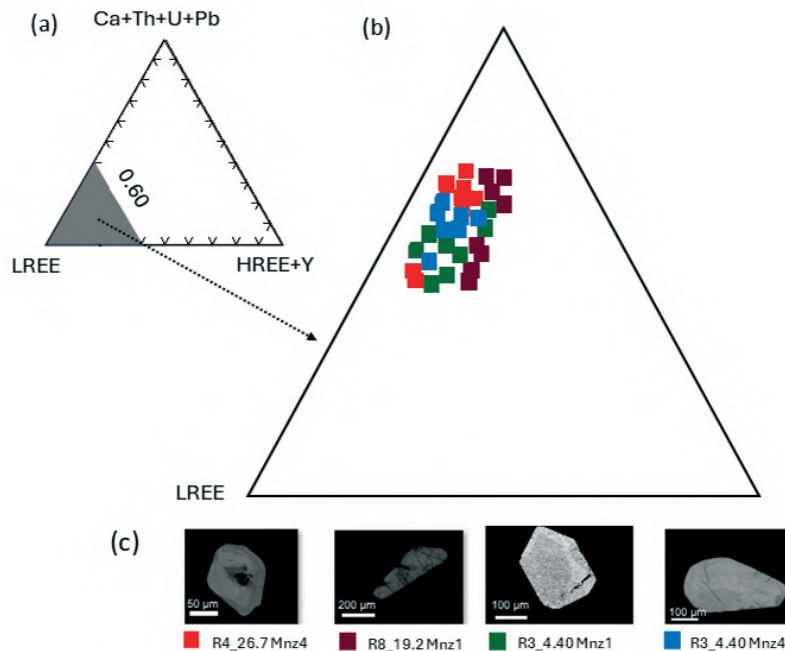
4.2.5. Monazite

Monazite in the Grt-ASMG and Bt-Sil-Gn samples occurs in fine-grained clusters and as inclusions within garnet and biotite. In contrast, most monazite in the Mnz-PTT dikes occurs as large crystals (> 200 μm) with complex chemical zoning, visible in backscatter electron microscope (BSE) imaging, while a minority exhibit homogenous or weak zoning. Most monazite grains from Mnz-PTT contain high concentrations of LREE and Ca, Th, U, Pb and lower HREE (Fig. 7). Minute grains of a $ThSiO_4$ mineral, probably thorite, are commonly closely associated with monazite grains. The concentrations of Th and U are at a level common for granitic rocks and vary only in a narrow interval ranging from 14.9 to 20.2 wt.% ThO_2 and from

0.2 to 1.2 wt.% UO_2. The Si and Ca contents range from 2.6 to 4.0 wt.% SiO_2 and 0.7 to 1.1 wt.% CaO, and indicate that Th is partially incorporated into the monazite structure due to substitution of both thorite $(Th,U)SiO_4$ and cheralite $Ca(Th,U)(PO_4)_2$ (Electronic Appendix 5).

BSE images of monazite grains in sample R3_4.40 reveal core to rim or patchy zoning with irregular domains of variable composition (Fig. 8a). The monazite grains typically display an irregular core- to rim chemical zoning, characterized by two distinct domains, a lighter Th-rich core and a darker Th-poor marginal overgrowth. The core is cut by a zone that has less Th which probably is caused by dissolution and recrystallization (Fig. 8 b, c, d). U and Y contents are almost uniform in both core and rim, because monazite generally contains less than 1 wt. % UO_2 and Y_2O_3. However, some monazites exhibit small U-and Y-rich zones towards the rim (Fig. 8e, f). EMPA data of selected monazite grains from Mnz-PTT sample R3_4.40 are characterized by (Electronic Appendix 5) high

Figure 7. (a) Ternary diagram illustrating the end-member composition of monazite in terms of LREE, HREE and Ca+Th+U+Pb, (b) Enlarged view of the ternary field showing monazite compositions from monazite-bearing tonalite-trondhjemite (Mnz-PTT) dikes, (c) BS images of selected monazite grains exhibiting concentric and patchy zoning, indicative of a history involving dissolution and replacement reactions.

ThO_2 (16.4–19.6 wt. %), low UO_2 (0.2–0.3 wt. %) and Y_2O_3 (0.73–0.96 wt. %) with dominant total REE of (49.9–52.8 wt. %). In these grains, the monazite end member varies between 76–79 mol. %, huttonite 14–17 mol. %, and cheralite 6–9 mol. %. Taken together, textural evidence and EMPA results suggest that these monazites can be assigned to a composition of monazite–huttonite/thorite solid solution that crystalized as early magmatic phases rather than forming as metamorphic porphyroblasts (Al-Ani et al. 2019).

4.3. Whole rock geochemistry

The whole-rock major and trace element data for the major lithologic phases of KGC; garnet-monzogranite (Grt-ASMG), Th-rich Mnz-PTT dikes and biotite-sillimanite gneiss (Bt-Sil-Gn) are presented in Electronic Appendix 7. The granitoids

in the Kovela area display a wide mineral modal range from alkaline granite to tonalite which is reflected in large geochemical variations (Fig. 9 and 10).

4.3.1. Garnet alkaline syeno-monzogranite-granodiorite (Grt-ASMG)

Harker diagrams show quite distinct trends for the two lithological units Grt-ASMG and Mnz-PTT (Fig. 9). Grt-ASMG samples are mostly distributed along more or less linear trends (Fig. 8), showing a negative correlation of Al_2O_3, Na_2O, K_2O, $FeO_{(t)}$ MgO, MnO, and P_2O_5 with SiO_2 while CaO and TiO_2 have the opposite trend (Fig. 9f, g). In the K_2O-SiO_2 diagram, the Grt-ASMG samples are essentially high-potassic to shoshonite. The Grt-ASMG and Bt-Sil-Gn samples have high SiO_2 (68.3–79.5 wt.%), while Mnz-PTT samples
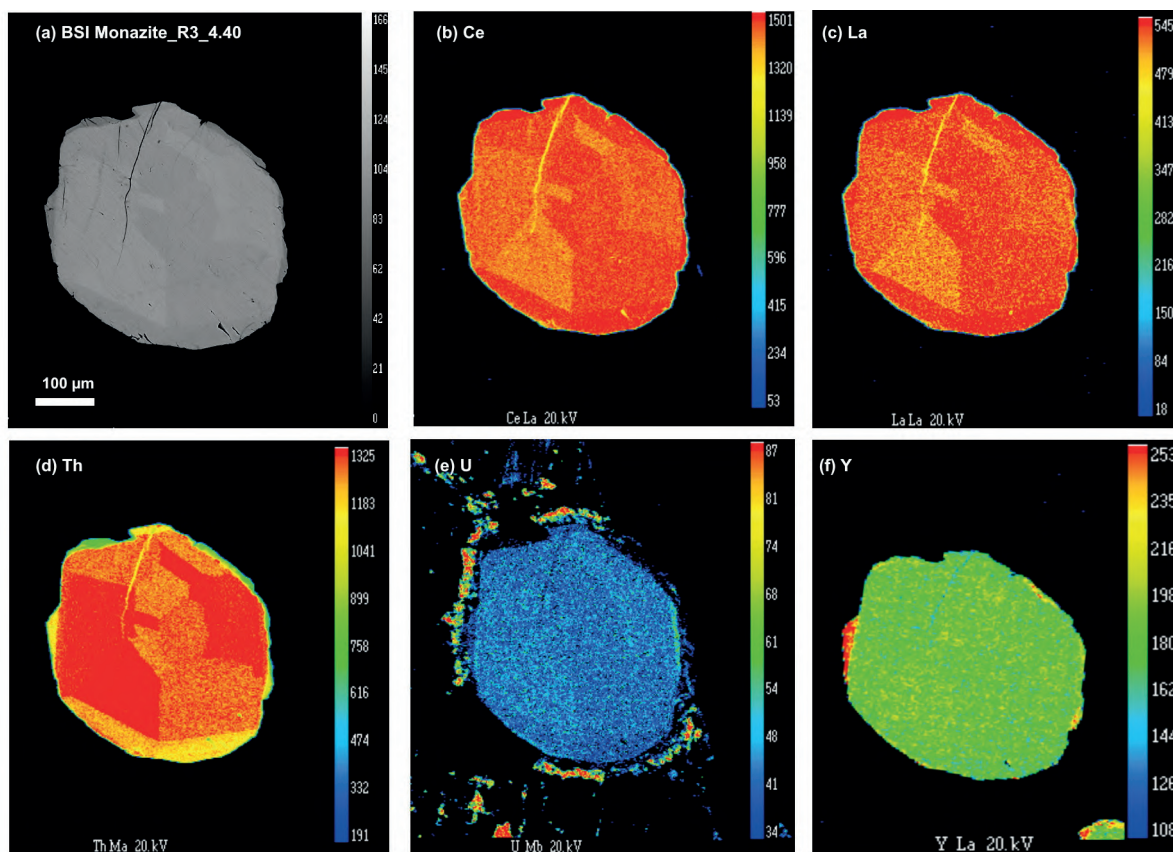
Figure 8. BSE image (a) and chemical maps (b–f) of a monazite grain from Th-rich monazite pegmatitic tonalite-trondhjemite dike (Mnz-PTT) sample R3_4.40: (a) backscatter electron (BSE) images of monazite characterized by patchy zoning with irregular compositional domains, (b–f) chemical maps of Ce, La, Th, U and Y, respectively.

are characterized by intermediate SiO_2 contents of 61.0–71.2 wt.%. In the K_2O-SiO_2 diagram (Fig. 9e), the Grt-ASMG samples plot in the shoshonite to calc-alkaline fields, compared to Mnz-PTT samples that are mainly calc-alkaline with one sample in tholeiitic field (Peccerillo and Taylor 1976).

Grt-ASMG rocks comprise mainly monzogranite and granodiorite, the monzogranite rocks are not discriminated between alkaline, syeno- and monzogranite using the QAP diagram (Fig. 10a; Streckeisen 1976). However, the Q-ANOR (CIPW normative, wt.%) diagram shows that the Grt-ASMG rocks (Fig. 10b) plot in these three fields and additionally in the granodiorite field (Streckeisen & Le Maitre 1979). The pink coarse-grained porphyritic granite, composed mainly of potassium feldspar and quartz with minor amounts of plagioclase and biotite is alkaline granite. Garnet is the dominant accessory mineral with minor zircon and Ti-Fe oxide (Fig. 3a). The syenogranite occurs as pink, fine-to coarse-grained massive to foliated rocks (Fig. 3b), but it has less K-feldspar and quartz, and a higher content of plagioclase, biotite and garnet relative to alkaline granite. The monzogranite occurs as a grey, medium-to coarse-grained rock (Fig. 3c). It is composed mainly of plagioclase and quartz with low contents of K-feldspar and biotite relative to the alkaline granite. The Grt-ASMG rocks have a high SiO_2 (69.79–79.50 wt.%), average Al_2O_3 content (11.80–17.10 wt.%), are alkali-rich with K_2O+Na_2O contents of 5.34–10.64 wt.%

and K_2O/Na_2O ratios ranging from 0.20 to 2.82, a moderate amount of CaO (0.35–2.21 wt.%), and small amounts of MgO, MnO and TiO_2. In the $FeO_{tot}/(FeO_{tot} + MgO)$ vs. SiO_2 (wt.%) discrimination diagram of Frost and Frost (2008), the Grt-ASMG samples are ferroan alkali granites. They show peraluminous character with A/CNK (molar $Al_2O_3/(Na_2O + K_2O + CaO)$) values between 1.04 to 1.34 and A/NK (molar $Al_2O_3/(Na_2O + K_2O)$) values between 1.49 to 2.51 (Fig. 10c, d).

The Grt-ASMG samples are characterized by low total REE contents (20–166 ppm) and low $(Ce/Yd)_n$ ratios (1.4–9.7) with a negative Eu anomaly (Eu/Eu*= 1.6–34.2) (Fig. 11a). The primitive mantle -normalized trace element patterns are LILE-enriched, show positive anomalies for Rb, K, Th, U, and Zr while Ba, Sr, Nb, REE, and Y show negative anomalies (Fig. 11b).

4.3.2. Th-rich monazite pegmatitic tonalite-trondhjemite dikes (Mnz-PTT)

The SiO_2 content of the Mnz-PTT samples is slightly lower than in the Grt-ASMG and Bt-Sil-Gn samples. As such, they are richer in Al_2O_3, CaO, and Na_2O and poorer in K_2O, leading to higher A/NK and A/CNK ratios that correspond to strongly peraluminous compositions. On the QAP diagram (Streckeisen 1976), the Mnz-PTT samples plot in the tonalite field and one sample plots in the quartz monzonite field (Fig. 10a). These samples are composed mainly of plagioclase (46.5–81.7 vol.%), alkali feldspar (4.5–28.5 vol.%) and quartz (6.5–38.8 vol.%). Other minerals (and their vol.%) include biotite (0.2-0.6), apatite (0.1–2.6), iron oxide (0.3–1.2), with zircon and monazite in trace amounts. According to the Q-ANOR (CIPW normative, wt.%) diagram, the Mnz-PTT samples plot within the field of tonalite to quartz diorite, while only one sample that plots in the quartz syenite field (Fig. 10b).

The REE patterns of the KGC granitoid groups differ significantly (Fig. 11a), with Mnz-PTT

samples showing substantial REE enrichment (REE_{Tot} from 1332 to 42 072 ppm) compared to Grt-ASMG samples (REE_{Tot} 35–60 ppm). This trend is also evident in the REE vs. P_2O_5 diagram (Fig. 9i), which highlights the abundance of monazite in various rock types. Moreover, the studied samples have significant negative Eu anomalies (Eu/Eu* = 0.01–0.05, 0.11–0.36, and 0.06–0.13; for Mnz-PTT, Grt-ASMG and Bt-Sil-Gn, respectively), suggesting significant plagioclase removal. The primitive mantle normalized trace element diagrams show common features such as distinct Ta, Nb, Ti, Ba, and Sr troughs and enrichment in Th, Rb, P, U, and LREE (Fig. 11b).

4.3.3. Biotite-sillimanite gneiss (Bt-Sil-Gn)

The result of the whole-rock chemistry of Bt-Sil-Gn samples show a SiO_2 range of between 68.30–78.80 wt.%, Al_2O_3 content range from 9.33–17.20 wt.%, while MgO and $FeO_{(tot)}$ are between 0.25–1.47 wt.% and 0.52–5.46 wt.%, respectively (Electronic Appendix 7). The Bt-Sil-Gn samples are lowest in Na_2O, K_2O and CaO but have high FeO (tot) and MgO contents and higher FeO_{Tot}/MgO ratios (0.15–2.55) than Grt-ASMG and Mnz-PTT. The Bt-Sil-Gn rocks, derived from supracrustal sources, are characterized by elevated Fe and Mg contents and low alkali contents. As a results, they are not included in geochemical classification diagrams of granitic samples Grt-ASMG and Mnz-PTT.

4.4. Pressures and temperatures

The peak metamorphic P–T conditions of the major lithologic phases of the KGC were quantified by conventional geothermobarometry. Temperatures were calculated based on experimental and empirical calibrations of Fe–Mg exchange between garnet-biotite pairs (GB) (Holdaway, 2000). The garnet-plagioclase-biotite-quartz (GPBQ)
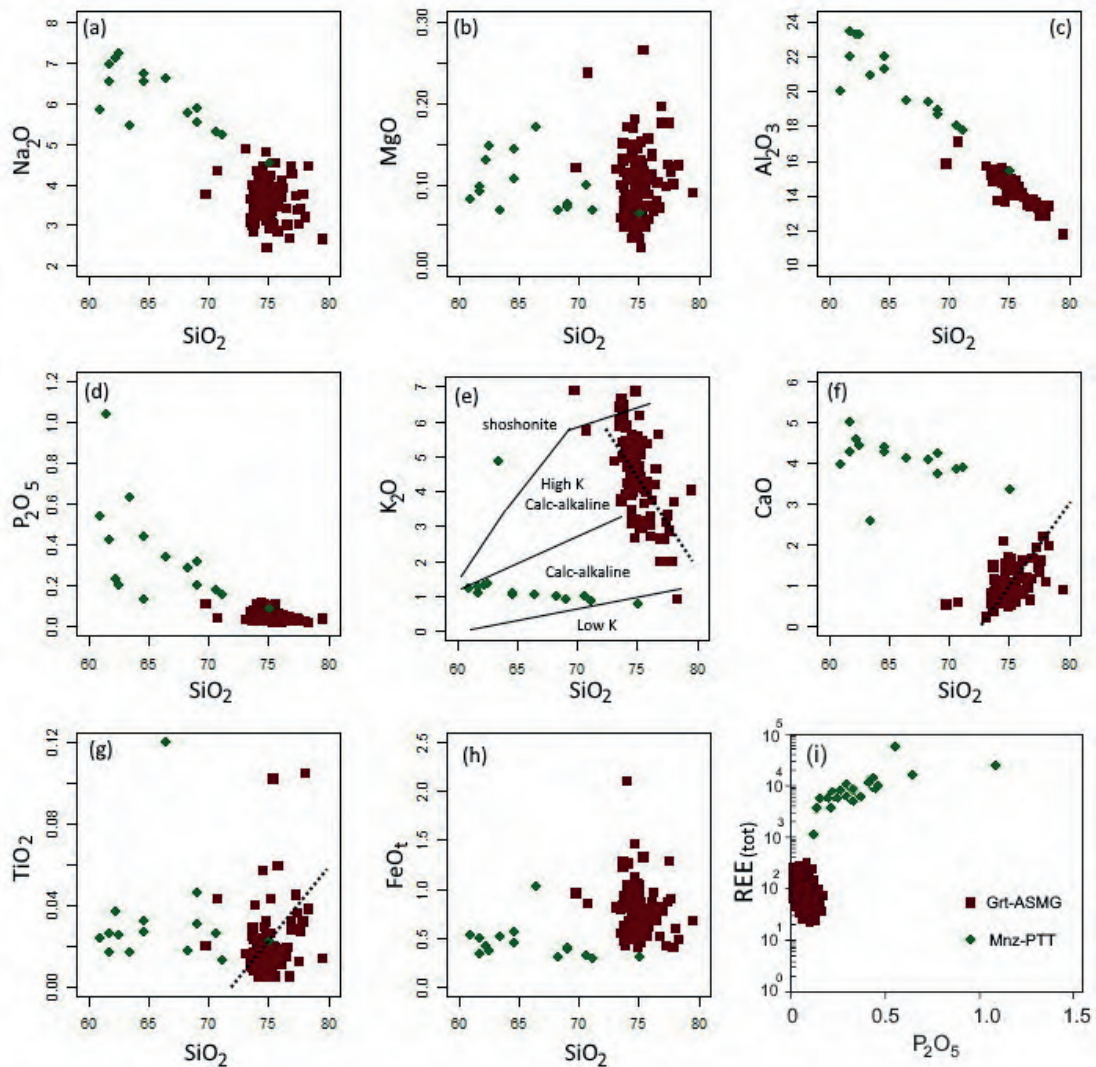
Figure 9. Harker diagrams for major and trace elements illustrating the geochemical trends of the magmatic rocks in KGC. The dashed lines highlight general geochemical trends observed in terms of SiO_2 with CaO and TiO_2, respectively.

geobarometry based on experimental calibration (Wu et al. 2004) was applied to constrain the peak metamorphic pressure for the studied rocks. According to the authors, the geothermobarometric estimates have minimum errors of ± 25 °C and ± 0.5 kbar. The calculated results are listed in Electronic Appendix 6 and in Table 1. The composition of garnet (core as well as rim) has been paired with the compositions of matrix biotite and matrix plagioclase to calculate inferred P–T peak conditions using

GB-GPBQ geothermobarometers. Results of the geothermobarometers for the five samples (Table 1) show that all three rock types plot within the sillimanite stability field (Fig. 12).

The estimated garnet core temperature in this case is the highest due to its Mg-rich composition, while the rim temperature reflects the late cation exchange during cooling. In the Grt-ASMG sample R2_17.30, the maximum temperature and pressure recorded at the grain cores are 770 °C and 3.9 kbar, respectively, whereas the minimum
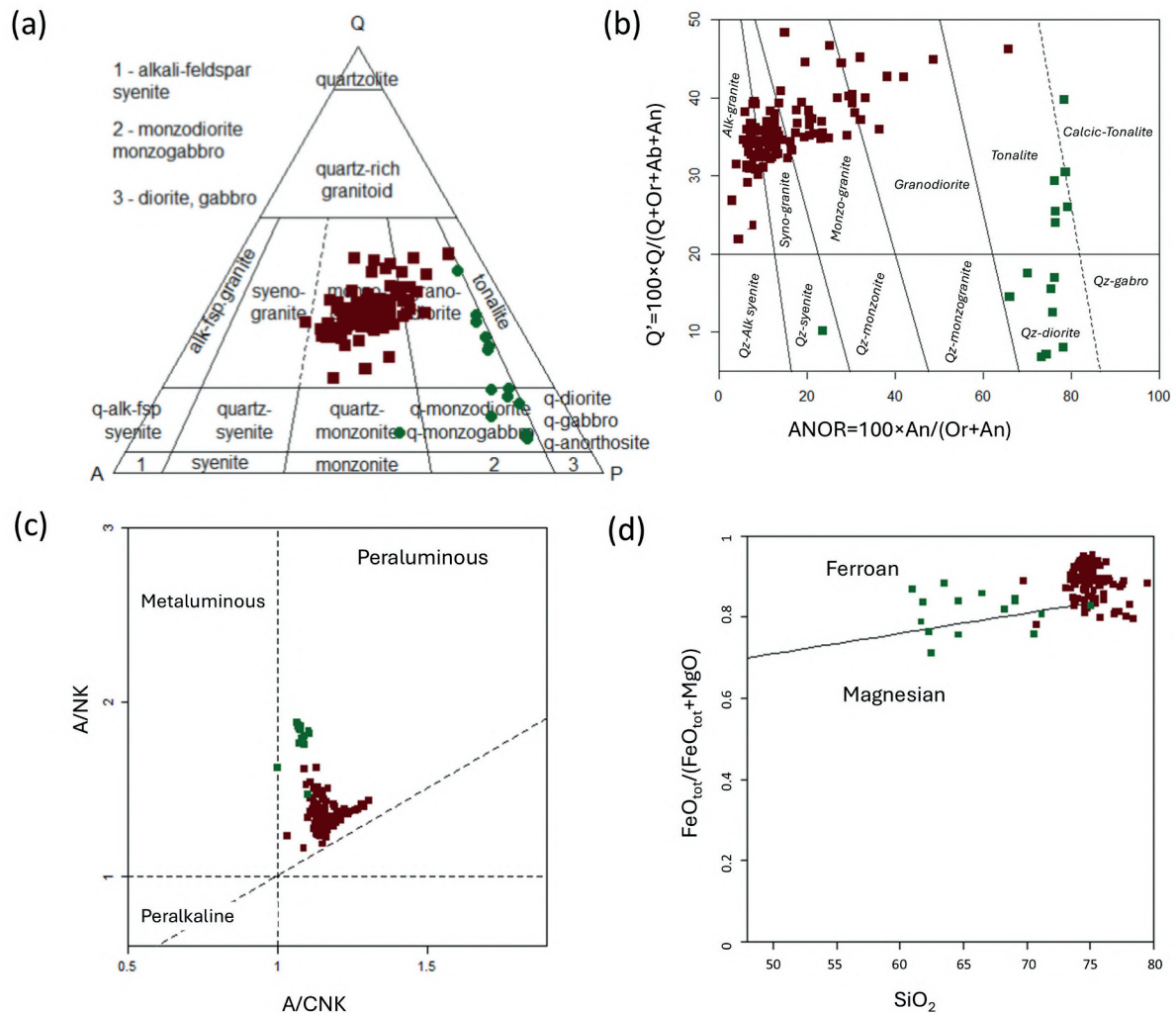
Figure 10. Geochemical plots of samples from the KGC. (a) QAP (IUGS, Modal, Vol%) classification diagram for magmatic rocks in KGC (Streckeisen 1976), Q=Quartz, A=Alkali feldspar, P=Plagioclase. (b) Q'-ANOR normative composition diagram (Streckeisen & Le Maitre 1979), AN= Anorthite, OR= Orthoclase. (c) A/NK versus A/CNK plot (Maniar and Picooli, 1989). (d) $FeO_{tot}/(FeO_{tot} + MgO)$ vs. SiO_2 (wt.%) discrimination diagram of Frost and Frost (2008).

values at the rims are 600 °C and 4.2 kbar (Fig. 12). For Mnz-PTT samples, the maximum temperatures calculated using the averages of garnet core compositions are: 1. sample R3_0.5, 718 °C (sd 43 °C) at 4.3 kbar (sd 0.9 kbar) and 2. sample R8_18.50, 643 °C (sd 4 °C) at 4.1 kbar (sd 0.4 kbar). For the Bt-Sil-Gn sample R1_29.75, the average core temperature is 753 °C (sd 12 °C) at a pressure of 4.8 kbar (sd 1.6 kbar).

4.5. Geochronology

The age determination results of representative samples of the KGC are summarized in Table 2. The monazite and zircon U-Pb data for eight selected samples are given in Electronic Appendix 8. Samples for age determinations were selected from the three main rock types of KGC: Grt-ASMG, Bt-Sil-Gn) and Mnz-PTT.
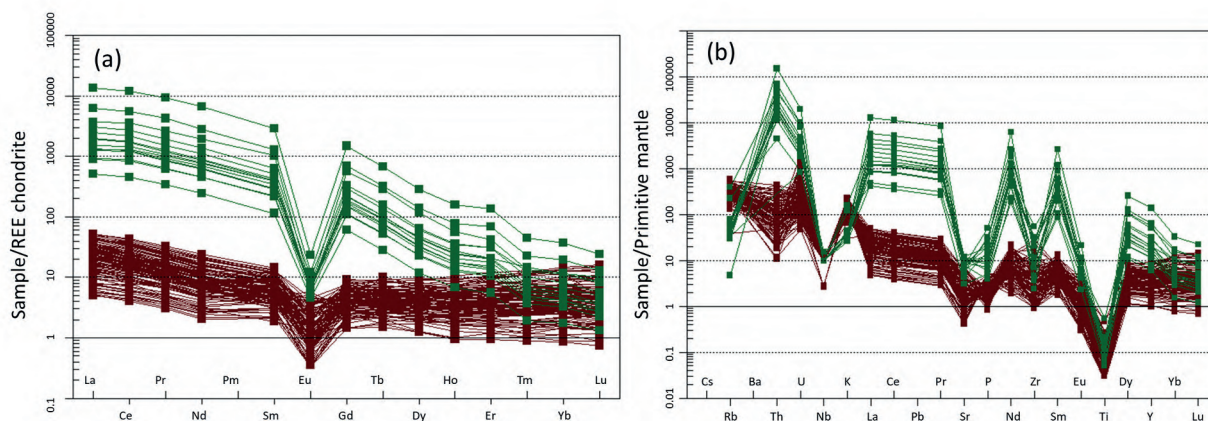
Figure 11. (a) Chondrite-normalized REE distribution patterns, (b) Primitive mantle -normalized trace element diagrams of KGC granitoids. Normalization factors are from McDonough and Sun (1995). Symbols as in Fig. 10.

Sample		avT	sd(T)	avP	sd(P)	corr
R1 29.75		753	12	4.8	1.6	0.922
R3_0.50		718	43	4.3	0.9	-0.500
R8 18.50		643	4	4.1	0.4	0.883
R2_17.30		770	16	3.9	0.1	0.869
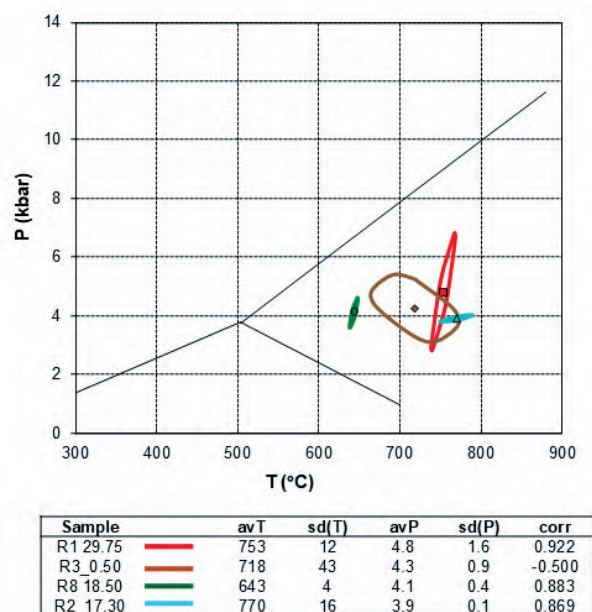
Figure 12. P-T diagram showing the peak-metamorphic conditions of the major lithologic phases of KGC. And = andalusite, Ky = kyanite, Sil = Sillimanite. Plot points inside the error ellipse represent the average P-T conditions, calculated using the average garnet core composition from multiple analysis points, based on the Holland & Powell (1990) program and dataset with correlated uncertainties.

4.5.1. Garnet-alkaline-syeno-monzogranite-granodiorite (Grt-ASMG)

U-Pb dating on monazite and zircon were made from two samples R2_17.3 and R8_40.7. These samples all contain a small amount of monazite and zircon grains, often found as inclusions in feldspar and quartz. The monazite grain size is mostly < 100 μm in diameter and the grains are irregular in shape, while zircon grains are rounded to elongated and typically 80–150 μm in diameter. Figure 13a shows the results for zircon from sample R2_17.3, displaying a high degree of discordance due to significant Pb loss. The data are scattered and do not yield any good age approximation for the rock. Three monazite grains from the same polished section give $^{207}Pb/^{206}Pb$ ages of 1886, 1915, 1925 Ma (mean = 1908 ± 48 Ma) and a concordia age of 1909 ± 18 Ma, providing an age estimate either for the initiation of magmatism in the KGC or a significant metamorphism at that time.

The polished thin section of gneiss sample R8_40.7 contained a few grains of zircon and monazite. The zircons are highly discordant (Fig. 13b), have very low $^{206}Pb/^{204}Pb$ ratios (<200), low Th contents and are therefore almost certainly

Table 1. Average electron microprobe analyses for garnet, biotite and plagioclase compositions in addition to the temperatures and pressures estimated by the GB thermometer and GBPQ barometer.

| Sample	R1 29.75_Grt 1_Rim			R1 29.75_Grt 1_Core			R3_0.5_Grt 2_Rim			R3_0.5_Grt 2_Core		
Mineral	Gr_rim	Bt matrix	Pl matrix	Gr_Core	Bt inclusion	Pl inclusion	Gr_rim	Bt matrix	Pl matrix	Gr_Core	Bt inclusion	Pl inclusion
SiO_2	36.79	34.42	65.14	37.49	35.33	66.75	35.96	31.66	61.33	36.16	30.08	60.43
TiO_2	0.00	0.05	0.00	0.00	0.09	0.00	0.04	2.89	0.00	0.02	2.76	0.04
Al_2O_3	20.56	20.99	21.05	20.94	22.67	20.52	20.68	19.20	23.14	20.82	18.73	23.29
FeO^T	35.18	21.41	0.18	34.66	20.57	0.16	36.76	24.90	0.02	36.13	26.63	0.04
MnO	4.12	0.25	0.02	2.64	0.25	0.00	2.46	0.17	0.01	2.05	0.18	0.00
MgO	2.15	7.51	0.00	3.92	6.01	0.00	2.22	5.95	0.05	2.85	6.39	0.03
CaO	0.97	0.00	4.09	0.96	0.01	3.41	1.07	0.23	5.01	1.42	0.14	5.55
Na_2O	0.00	0.00	9.92	0.00	0.00	9.17	0.00	0.00	8.52	0.00	0.00	8.53
K_2O	0.00	9.20	0.10	0.00	9.54	0.12	0.00	9.54	0.27	0.00	9.20	0.37
O calc.	12.00	22.00	8.00	12.00	22.00	8.00	12.00	22.00	8.00	12.00	22.00	8.00
Si	2.21	4.02	2.59	2.23	4.10	2.66	2.17	3.67	2.49	2.18	3.52	2.46
Ti	1.64	3.27	1.11	1.66	3.51	1.09	1.66	2.97	1.25	1.67	2.92	1.26
Al	0.00	0.01	0.00	0.00	0.01	0.00	0.00	0.34	0.00	0.00	0.32	0.00
Fe	4.22	5.01	0.01	4.12	4.78	0.01	4.44	5.78	0.00	4.35	6.23	0.00
Mn	0.49	0.06	0.00	0.31	0.06	0.00	0.30	0.04	0.00	0.25	0.04	0.00
Mg	0.26	1.76	0.00	0.47	1.40	0.00	0.27	1.38	0.00	0.34	1.49	0.00
Ca	0.12	0.00	0.33	0.11	0.00	0.27	0.13	0.05	0.41	0.17	0.03	0.45
Na	0.00	0.00	1.58	0.00	0.00	1.46	0.00	0.00	1.38	0.00	0.00	1.39
K	0.00	4.30	0.02	0.00	4.43	0.02	0.00	4.43	0.04	0.00	4.30	0.06
Formulae and endmembers of garnets												
XFe	0.787			0.755			0.820			0.796		
XMg	0.088			0.157			0.091			0.115		
XCa	0.029			0.027			0.032			0.041		
XMn	0.096			0.060			0.057			0.047		
GB-GBPQ temperature °C and pressure Kbar calculations												
T °C	622			766			686			777		
Kbar	5.1			6.4			3.2			3.3		

of hydrothermal origin. A poorly constrained [207]Pb/[206]Pb age of 1718 ± 44 Ma can be calculated from these data. Three monazite grains in the same polished section provide [207]Pb/[206]Pb ages of 1755, 1762, 1778 Ma (Concordia age = 1772 ± 13 Ma). These young ages attest to a metamorphic event significantly after the crystallization of the monzogranite.

4.5.2. Biotite-sillimanite gneiss Bt-Sil-Gn)

Bt-Sil-Gn contains 50–100 µm, rounded to subrounded grains of monazite and 100–300 µm long, prismatic, subhedral to subrounded zircon grains. U–Pb dating on monazite and zircon were made from sample R9_23.20. Monazites from the sample R9_23.20 are rich in Th, and the [207]Pb/[206]Pb

Table 2. Summary of the U–Pb age determinations for the KGC.

Sample	Coordinates	Monazite (Ma)	Zircon (Ma)
Mnz-PTT		$^{207}Pb/^{206}Pb$	
R3_4.40	N67 ° 02.031 E33 ° 26.850	1877–1781	
R4_29.30	N67 ° 01.670 E33 ° 27.036	1881–1813	
R8_18.5	N67 ° 02.080 E33 ° 26.798	1885–1796	1816±15
Bt-Sil-Gn			
R9_23.20	N67 ° 01.981 E33 ° 26.849	1816±7	1795±190
Grt-ASMG			
R2-17.3	N67 ° 02.030 E33 ° 26.864	1925-1886	1863±110
R8_40.7	N67 ° 02.080 E33 ° 26.798	1778-1755	1718±44
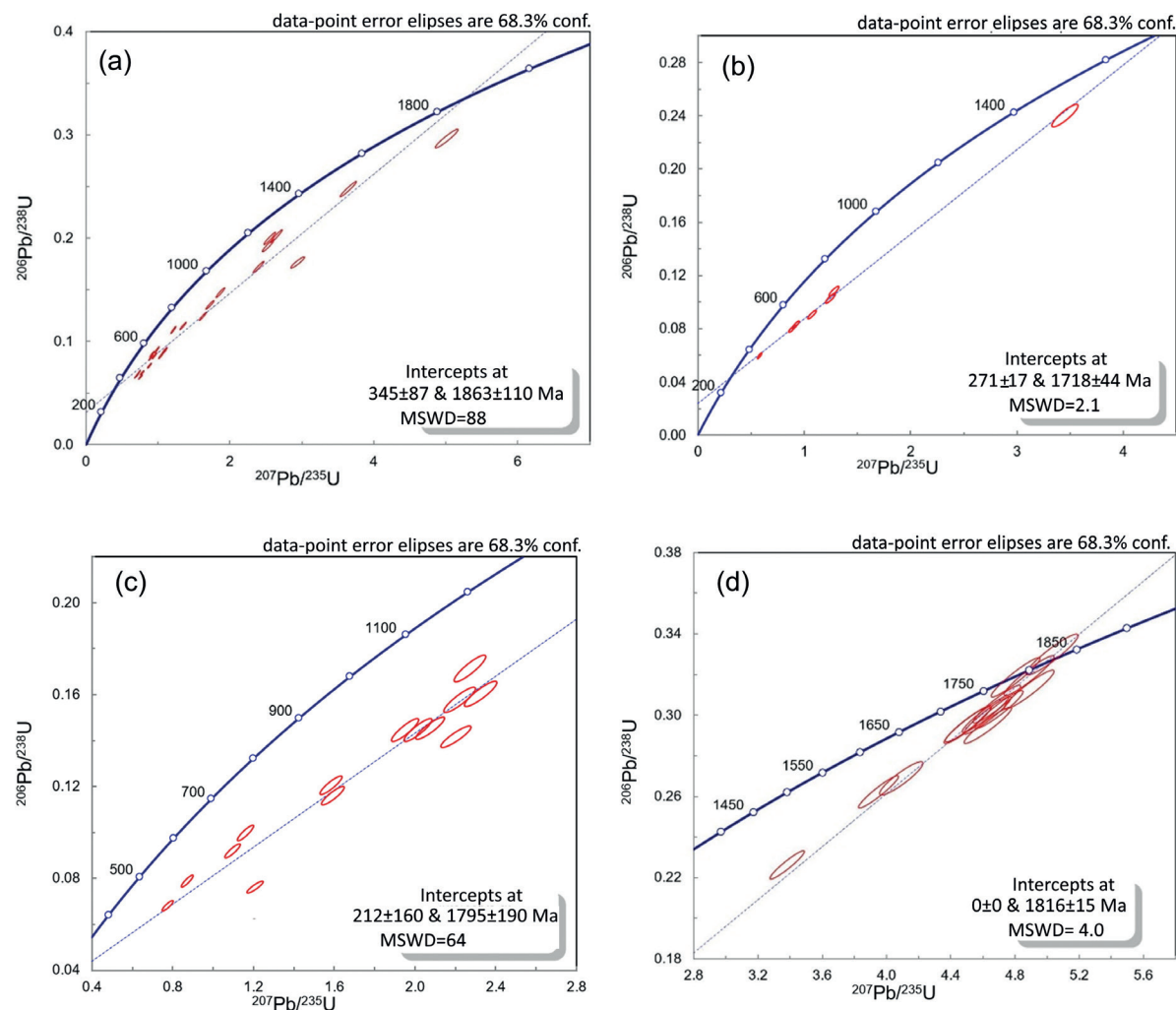
Figure 13. U-Pb concordia diagrams of granite intrusions in KGC. (a, b) U-Pb zircon concordia plots of Grt-ASMG samples R2_17.3 and R8_40.7, respectively (c) U-Pb zircon concordia plot for Bt-Sil-Gn sample R9_23.20, (d) U-Pb zircon concordia plot for Mnz-PTT sample R8_18.50.
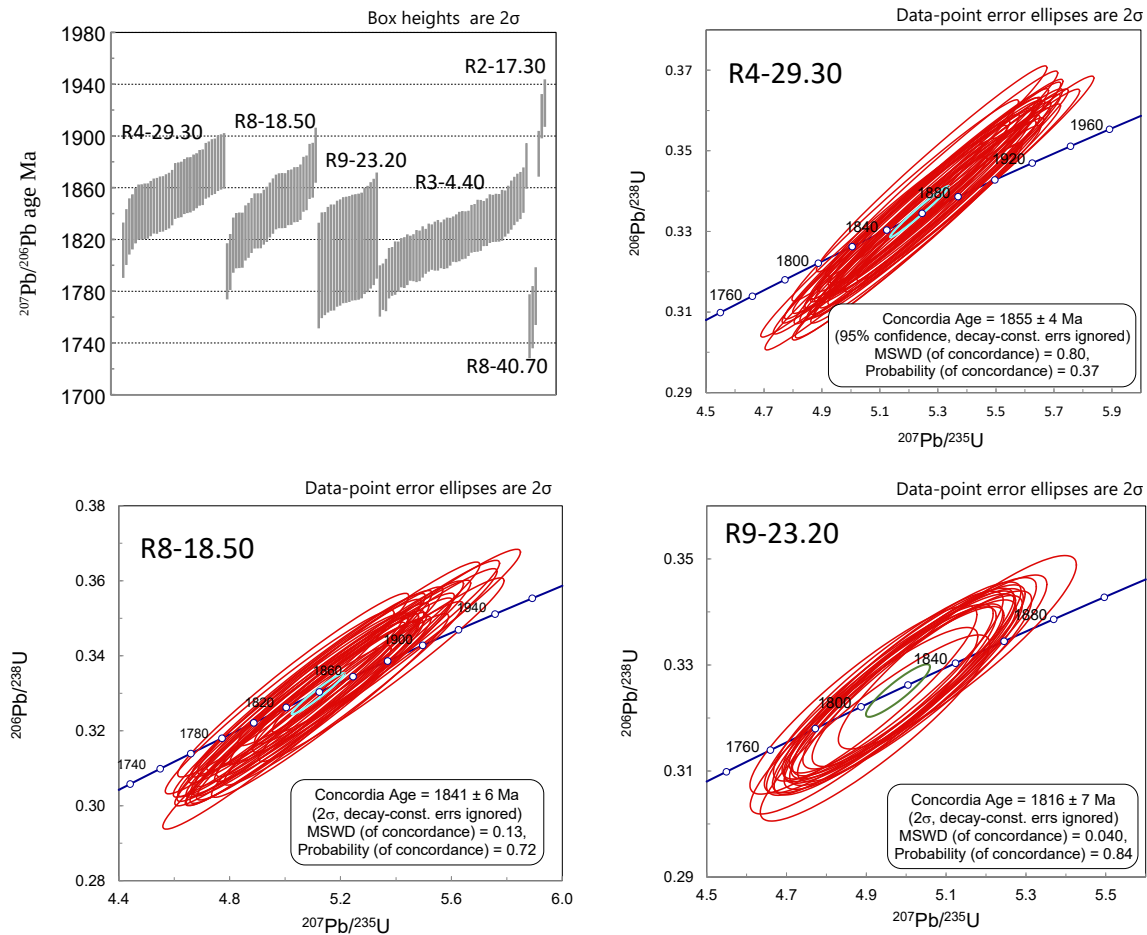
Figure 14. (a) Average ^{207}Pb/^{206}Pb ages of zircon from Kovela Granite Complex (KGC) samples (a) and U-Pb concordia diagrams for monazite in the dated samples, (b) sample R9_23.20, (c) sample R8_18.50, (d) sample R9_23.20.

ages do not differ much from each other. A robust concordia age of 1816 ± 7 Ma could be calculated for this sample (Fig. 14d). In contrast, zircons from the same polished section have very low ^{206}Pb/^{204}Pb ratios suggesting they have been affected by hydrothermal fluids, and consequently provide a very poorly constrained age of 1795 ± 190 Ma (Fig. 13c).

4.5.3. Monazite-rich pegmatitic tonalite-trondhjemite dikes (Mnz-PTT)

The investigated Th-rich dikes contain monazite that forms complexly zoned subhedral to euhedral crystals variable in size (200 – 1500 µm in diameter) and characterized by weak concentric and patchy zoning. Transmitted light photomicrography and BSE imaging of monazite grains was described in Al-Ani et al. (2019). Two robust ages were produced from samples of this rock type. Sample R8_18.50 contains abundant large monazites which produced

concordant U-Pb data. The data show a rather continuous spread of ^{207}Pb/^{206}Pb ages from 1796 to 1885 Ma. The 2σ errors are high (20 Ma), but the oldest and youngest ages clearly differ from each other, considering the error limits. However, a concordia age of 1841 ± 6 Ma can be calculated for this sample (Fig. 14c). Zircon in the same sample yielded an upper intercept age of 1816 ± 15 Ma (Fig. 13f). In this sample, there are a two zircon grains whose ^{207}Pb/^{206}Pb age is 1.8–1.85 Ga that may be inherited. In the dike sample R4_29.30, the ^{207}Pb/^{206}Pb ages are from 1813–1881 Ma (Fig. 14a, b). The sample yielded a concordia age of 1855 ± 4 Ma (Fig 14c). Sample R3_4.40 contains monazites with concordant or near-concordant ^{207}Pb/^{206}Pb ages ranging 1781–1877 Ma, with a rather continuous spectrum (Fig. 14a).

5. Discussion

5.1. Age determinations

The U-Pb data presented here show that there remain considerable uncertainties in the relative and absolute ages. However, the age distribution of monazites in the Kovela complex is very similar to that of the paragneisses and granitoids in the Sulkava granulite complex in eastern Finland (Salminen et al. 2022). Also in Sulkava c. 110 km northeast of Kovela, the oldest monazites in paragneisses are 1.92 Ga or even a bit older, and most dated samples both from metasedimentary rocks and granitoids show a continuous spread of monazite ^{207}Pb/^{206}Pb ages from 1.89 Ga to 1.78 Ga. Salminen et al. (2022) interpreted this age distribution so that the oldest ≥1.92 Ga grains would be detrital, then there were two high-grade metamorphic events at 1.89–1.86 Ga and 1.83–1.82 Ga, followed by late fluid infiltration at 1.80–1.77 Ga. The dates between these age peaks could have been caused by mixed isotopic ages in patchy grains, or alternatively, the crust stayed hot enough for monazite to crystallize during the following 100 Ma after 1.89 Ga.

The Svecofennian magmatism took place at 1.90–1.87 Ga, and the crust in southern Finland could have stayed hot for some 100 Ma before the final docking. The KGC did not yield reliable U-Pb ages on zircon that would give their crystallization ages. Concordia ages of 1.86 and 1.84 Ga could be calculated for the two Mnz-PTT samples, but these may be artefacts caused by the high analytical errors. On the other hand, Torvela and Kurhila (2022) observed 1.85 Ga titanites in granulite facies shear zones in Vihti, c. 25 km east of Kovela (Fig. 1). Because this age is difficult to link with any prominent thermal event in southern Finland, they interpreted these ages to represent either a mixed age or reflect a temporary cooling below the titanite U-Pb closure temperature (Torvela & Kurhila 2022). However, Kara et al. (2020) reported 1.86 Ga gabbro and adakite-like intrusions in southern Finland, and presumably a crustal heat flow was connected with this magmatism as well. The zircon and monazite age range is 1.85–1.79 Ga for the abundant S-type leucogranites in southern Finland that were produced in partial melting of the crust (Kurhila et al. 2005; Nironen & Kurhila 2008; Kurhila et al. 2011). These observations suggest that although the main phase of the Svecofennian magmatism took place at 1.90–1.87 Ga, the crust in Southern Finland could have stayed hot for some 100 Ma before the final docking. However, the Kovela granitoids could be older on the basis of their 1.88 Ga and even older monazites, but the 1816 Ma old monazite in the biotite-sillimanite gneiss xenolith is then a problem (Fig. 13). It is difficult to imagine a younger xenolith in an older intrusion, or why the monazite recorded only the 1.82 Ga metamorphism in the xenolith, although the host granitoid has a wide spread of monazite ages from 1.93 to 1.79 Ga. In the southern Finland the highest-grade metamorphic event, producing granulite and migmatite, has been dated at 1.84–1.80 Ga (Korsman et al. 1984; Kurhila et al. 2005; 2011; Mouri et al. 2005; Väisänen & Kirkland 2008; Salminen et al. 2022; Torvela & Kurhila 2022). The 1816 Ma monazite age in the Kovela xenolith fits well within these brackets.

Metasedimentary migmatite xenoliths are found also in the outcrops in Kovela, and they partly form the host rock of the granitoids. Therefore, the most probable interpretation is that the Kovela granitoids were emplaced into mid-crust during the late stage of the Svecofennian orogeny and crystallized at around 1.82 Ga. This interpretation is supported by the ~1.82 Ga zircon age obtained from the monazite-rich tonalite-trondhjemite dike sample R8_18.5, although the age uncertainty is relatively high.

The possible reason for the wide spread of the monazite ages in granitoids would be that the older monazites are inherited. In their experimental work, Van Lichtervelde et al. (2021) showed how small monazite grains are dissolved in peralkaline glass, while big grains are only partially dissolved and later recrystallized. Van Lichtervelde et al. (2021) also suggested that elevated phosphorus concentrations in the melt decreases monazite solubility. The high ThO_2 content (17–19 wt.%) of most monazite grains in the Kovela granitoids suggests that monazite is magmatic (Montel et al. 2018; Al-Ani et al. 2019). Therefore, the age spread of monazite in Kovela, especially in the P-rich Mnz-PTT dikes, is explained by crystallization of some monazite in the early stages of the magma development at around 1.88 Ga, followed by dissolution of the smaller grains and their continuous recrystallization during the subsequent evolution of the granitoid magmas. This would also mean that the parental melts of the pegmatites existed already at around 1.88 Ga.

5.2. Garnet megacrysts

The compositions of garnet megacrysts from the studied rock types also provide information about the classification of their host. Almandine-rich garnet in ASMG could be a product in the melting reactions that produced the parental melts of the pegmatites, or it could have been crystallized later from the pegmatite melts. In the granulite facies pelitic migmatites that surround the Kovela complex, MgO in garnet is generally 4–5 wt.%

(Fig. 5b), suggesting metamorphic temperatures of 700–800 °C (Schreurs & Westra 1986). Most garnet grains in the Kovela granitoids have MgO of 2–3 wt. % suggesting lower, <700 °C crystallization temperatures, being close to the wet solidus of pelitic compositions. Some garnet cores in Grt-ASMG are, however, richer in MgO, having values up to 4.2 wt. %, not far from the garnet compositions in the surrounding migmatites. These garnets are zoned so that in the rims the MgO decreases to 2–3 wt. %, indicating that garnet rims grew during decreasing temperature, or that their composition was changed by diffusion during cooling. Diffusion during slow cooling of the melt could have changed completely the composition of some garnet grains, which would explain the compositional differences, or alternatively garnet, like monazite, was crystallized during long periods, all grains not representing the same PT conditions. Consequently, the usage of garnet-based geothermobarometry should be considered with great caution in these kinds of igneous rocks.

5.3. Origin of the monazite-bearing tonalitic-trondhjemitic (Mnz-PTT) dikes

Although the magma source is considered to be the primary control on the geochemical composition of granitic rocks (e.g. Clemens & Stevens 2012), rock composition can also be influenced by magmatic processes such as partial melting, magma mixing, assimilation and fractional crystallization (e.g., Zheng & Gao 2021). The major elements and mineralogical signatures of studied rocks, show that there are two different compositional trends with little interaction between their magmas (Fig. 9–11). The CIPW normative AB–An–Or diagram (Fig. 10a) shows granite and granodiorite composition for the Grt-ASMG samples and tonalite to trondhjemite compositions for Mnz-PTT samples, respectively.

The REE and multi-element normalized

diagrams for the KGC lithologies show similar patterns for the Grt-ASMG samples, with relatively flat REE patterns. The HREE is quite high for granitic rocks which obviously is due to the presence of garnet in the analyzed samples (Fig. 11). The Mnz-PTT samples are rich in LREE and show highly fractionated REE. All patterns show distinct Nb, Ti, Zr, Sr, Ba and Eu* troughs and enrichment in Th and LREE.

The Grt-ASMG and Mnz-PTT differ compositionally so much from each other that they could have a different source. However, in many studies it has been demonstrated that liquid immiscibility plays an important role in the pegmatite petrogenesis (e.g. Müller et al. 2022; Thomas & Davidson 2008, 2013, 2014, 2016). Generally, pegmatites are thought to have been formed in granite fractionation where an alkali and H_2O rich residual melt is formed. Melt-melt-fluid immiscibility can take place in this residual, forming at least two immiscible melts, a relatively H_2O-poor peraluminous melt and an extremely H_2O-rich peralkaline melt. At the same time, other immiscible melts can be generated, or they can form during cooling. The process starts with the formation of small droplets that then coalesce into melt pools, forming separate melts because of the density and viscosity contrasts between the conjugate melts (Thomas & Davidson 2012, 2016). Moreover, many studies have shown that melt–melt immiscibility is an important mechanism in concentrating e.g. REE, U, and Th (Veksler et al. 2005; Vasyukova & Williamsjones 2014, 2016; Van Lichtervelde et al. 2021).

In their experiment with peralkaline glass and monazite-cheralite at 800 ºC and 200 MPa, Van Lichtervelde et al. (2021) observed the formation of immiscible droplets of melt that were strongly peraluminous, depleted in Si and K, enriched in P and F, and having high abundances of the monazite-cheralite constituents Ca, La, Eu, Th and U. Van Lichtervelde et al. (2021) argued that the Ca excess triggers the formation of a melt whose structure can accommodate large amounts of high field strength cations such as P, REE, U, and Th.

In Kovela, monazite is enriched in the tonalitic-trondhjemitic dikes whose CaO content is generally at least two times higher than that of the granitic-granodioritic host. Therefore, a possible process to form the monazite-rich dike is liquid immiscibility where tonalitic-trondhjemitic melts were separated from the granitic-granodioritic magma, accommodating elevated abundances of P, Th, and REE to form monazite.

On the map, the Kovela complex forms a dome-like structure where the mafic volcanic rocks wrap around the granite-granodiorite pluton (Fig. 2). Structural analysis of the area is lacking, but this kind of structure could represent a structural dome, like the Mustio dome c. 25 km south of Kovela (Bleeker & Westra 1987), or it could be a magmatic dome generated by the uprising granitoid magmas (Fig. 1).

5.4. Implications to the formation of the Kovela Complex

In summary, the development of the Kovela granitoid complex could be the following:

1. The melting of the metasedimentary source in upper mid-crustal levels at c. 1.88 Ga, coalescence of the granitoid magmas into pools.
2. Fractionation of the parental magma pools, forming H_2O-, REE-, and volatile-rich residues.
3. Liquid immiscibility of the residual magmas, forming the granite-granodiorite magmas and tonalite-trondhjemite magmas, gravity separation of the lighter granitic-granodioritic magmas from the heavier tonalitic-trondhjemitic magmas that gradually sink to the bottom of the pool.
4. Shortening and deformation, squeezing of the lighter granitic magmas to an existing structural dome, or generation of a magmatic dome at c. 1.82 Ga, followed by the intrusion of the tonalitic-trondhjemitic magmas from lower levels of the magma chambers,

intruding both the granite-granodiorite and its country rocks.

6. Conclusions

1. The geochemical data of the KGC reveals two compositionally different granitoid phases. The Grt-ASMG is granitic-granodioritic and the Mnz-PTT dikes are tonalitic-trondhjemitic. Both are peraluminous, with the latter showing a strong REE enrichment, higher A/NK & A/CNK ratios, and more pronounced negative Eu anomalies — features indicative of advanced magmatic differentiation including liquid immiscibility.

2. Thermobarometry indicates that garnet in the KGC rocks crystallized under high-temperature (640–770 °C) and low pressure (4–5 kbar) in similar PT conditions with the granulite facies migmatites that surround the KGC complex. This suggests that the melting producing the Kovela granitoids and their subsequent crystallization took place at the same crustal depths as the high-grade regional metamorphism of the country rocks.

3. LA-ICP-MS zircon and monazite U-Pb data indicates a prolonged evolution of the KGC. The oldest monazites in the granitoids are 1.93 Ga, and then monazite crystallized almost continuously from 1.88 Ga to final cooling at 1.76 Ga. The zircon age of 1.82 Ga in a Mnz-PPT dikes evidently records its emplacement.

Acknowledgments

Authorship contribution statement

T. Al-Ani – field work, sample selection and preparation, image processing, petrography, mineralogical analyses (SEM & EMPA), whole-rock geochemistry, conceptualization, interpretation, writing; P. Hölttä – field work, sample selection, thermobarometry, geochronology, conceptualization, interpretation, writing; H. O'Brien – sample selection for dating, U-Pb zircon & monazite age determinations, interpretation, writing of the geochronology section; K. Cutts – geothermometry, geobarometry, interpretation, writing.

Supplementary Data

Electronic Appendices 1–9 of the article are available via Bulletin of the Geological Society of Finland web page. Electronic appendices 1–6: Mineral chemistry analysis and geothermobarometric results. Electronic appendices 7: Major element (wt.%), trace element (ppm) and mineral composition of the studied KGC rocks. Electronic Appendix 8. Detailed results of the zircon and monazite grain U-Pb geochronology, and description of dating by LA-ICP-MS. Electronic Appendix 9: Images of garnet megacrysts and mineral compositions.

References

Al-Ani, T., Hölttä, P., Grönholm, S., Pakkanen, L. & Al-Ansari, N., 2019. Crystal Chemistry and Geochronology of Thorium-Rich Monazite from Kovela Granitic Complex, Southern Finland. Natural Resources 10, 230–269. https://doi.org/10.4236/nr.2019.106016.

Andersson, U. B. & Öhlander, B., 2004. The late Svecofennian magmatism. In: Högdahl, K. et al. (eds), The Transscandinavian Igneous Belt (TIB) in Sweden: a review of its character and evolution. Geological Survey of Finland, Special Paper 37, pp. 102–104.

Bleeker, W. & Westra, L., 1987. The evolution of the Mustio gneiss dome, Svecofennides of SW Finland. Precambrian research, 36, 227–240. https://doi.org/10.1016/0301-9268(87)90022-2

Clemens, J. D. & Stevens, G. J. L., 2012. What controls chemical variation in granitic magmas? Lithos 134–135, 317–329. https://doi.org/10.1016/j.lithos.2012.01.001

Deer, W. A., Howie, R. A. & Zussman, J., 1992. An Introduction to the Rock-Forming Minerals, 2nd edition. Longman Scientific & Technical, London, 696 p.

Ehlers, C., Skiöld, T. & Vaasjoki, M., 2004. Timing of Svecofennian Crustal Growth and Collisional Tectonics in Åland, SW Finland. Bulletin of the Geological Society of Finland 76, 63–91. https://doi.org/10.17741/bgsf/76.1-2.004

Frost, B. R. & Frost, C. D., 2008. A Geochemical Classification for Feldspathic Igneous Rocks. Journal of Petrology 49, 1955–1969. https://doi.org/10.1093/petrology/egn054

Gaál, G. & Gorbatschev, R., 1987. An outline of the Precambrian evolution of the Baltic shield. Precambrian Research 35, 15–52. https://doi.org/10.1016/0301-9268(87)90044-1

Harangi, S. Z., Downes, H., Kósa, L., Szabo, C. S., Thirlwall, M. F., Mason, P. R. D. & Mattey, D., 2001. Almandine garnet in calc-alkaline volcanic rocks of the Northern Pannonian Basin (Eastern–central Europe): Geochemistry, petrogenesis and geodynamic implications. Journal of Petrology 42, 1813–1843. https://doi.org/10.1093/petrology/42.10.1813

Hawemann, F., Mancktelow, N. S., Pennacchioni, G., Wex, S. & Camacho, A., 2019a. Weak and slow, strong, and fast: How shear zones evolve in a dry continental crust (Musgrave Ranges, Central Australia). Journal of Geophysical Research: Solid Earth 123, 219–240. https://doi.org/10.1029/2018JB016559

Hawemann, F., Mancktelow, N. S., Wex, S., Pennacchioni, G. & Camacho, A., 2019b. Crystal plastic behavior of garnet under seismic stress in the dry lower continental crust (Musgrave Ranges, Central Australia) Solid Earth Discussions 10, 1635–1649. https://doi.org/10.5194/se-2019-110

Heilimo, E., Mikkola, P., Ahven, M., Huhma, H., Lahaye, Y. & Virtanen, V. J., 2023. Evidence of crustal growth during the Svecofennian orogeny: new isotopic data from the central parts of the Paleoproterozoic Central Finland Granitoid Complex. Precambrian Research 395, 107125. https://doi.org/10.1016/j.precamres.2023.107125

Holdaway, M. J., 2000. Application of New Experimental and Garnet Margules Data to the Garnet-Biotite Geothermometer, American Mineralogist 85, 881–892. https://doi.org/10.2138/am-2000-0701

Holland, T. & Powell, R., 1990. An enlarged and updated internally consistent thermodynamic dataset with uncertainties and correlations: the system K_2O–Na_2O–CaO–MgO–MnO–FeO–Fe_2O_3–Al_2O_3–TiO_2–SiO_2–C–H_2–O_2. Journal of metamorphic Geology 8, 89–124. https://doi.org/10.1111/j.1525-1314.1990.tb00458.x

Huhma, H., O'Brien, H., Lahaye, Y. & Mänttäri, I., 2011. Isotope Geology and Fennoscandian Lithosphere Evolution. In: Nenonen, K. & Nurmi, P. (eds.), Geoscience for Society: 125th Anniversary Volume. Geological Survey of Finland, Special Paper 49, pp. 35–48.

Huhma, H., Mänttäri, I., Peltonen, P., Kontinen, A., Halkoaho, T., Hanski, E. … & Whitehouse, M., 2012. The age of the Archaean greenstone belts in Finland. In: Hölttä, P. (ed.), The Archaean of the Karelia Province in Finland. Geological Survey of Finland, Special Paper 54, pp. 74–175.

Hölttä, P., Huhma, H., Lahaye, Y., Mänttäri, I., Lukkari, S. & O'Brien, H., 2020. Paleoproterozoic metamorphism in the northern Fennoscandian Shield: age constraints revealed by monazite. International Geology Review 62, 360–387. https://doi.org/10.1080/00206814.2019.1611488

Janoušek, V., Farrow, C. M. & Erban, V., 2006. Interpretation of whole-rock geochemical data in igneous geochemistry: Introducing Geochemical Data Toolkit (GCDkit). Journal of Petrology 47, 1255–1259. https://doi.org/10.1093/petrology/egl013

Jurvanen, T., Eklund, O. & Väisänen, M., 2005. Generation of A type granitic melts during the late Svecofennian metamorphism in south Finland. GFF 127, 139–147. https://doi.org/10.1080/11035890501272139

Kara, J., Väisänen, M., Heinonen, J. S., Lahaye, Y., O'Brien & Huhma, H., 2020. Tracing arclogites in the Paleoproterozoic Era–A shift from 1.88 Ga calc-alkaline to 1.86 Ga high-Nb and adakite-like magmatism in central Fennoscandian Shield. Lithos 372, 105663. https://doi.org/10.1016/j.lithos.2020.105663

Karvinen, S., Makkonen, H. V., Mikkola, P., Rämö, O. T., Huhma, H. & Niskanen, M., 2025. Mafic-ultramafic intrusions of Matokulma, Palojärvi, and Hongonniittu within the Central Finland Granitoid Complex with special reference to their petrogenesis and ore potential. Bulletin of the Geological Society of Finland 97, 31–64. https://doi.org/10.17741/bgsf/97.1.002

Kemp, A. I. S., Hawkesworth, C. J., Foster, G. L., Paterson, B. A., Woodhead, J. D., Hergt, J. M. & Whitehouse, M. J., 2007. Magmatic and crustal differentiation history of

granitic rocks from Hf-O isotopes in zircon. Science 315, 980–983. https://doi.org/10.1126/science.1136154

Kohn, M. J., 2003. Geochemical zoning in metamorphic minerals. In: Rudnick, R. L. et al. (eds.), Treatise on Geochemistry: The Crust. Elsevier–Pergamon, New York, pp. 229–261. https://doi.org/10.1016/B0-08-043751-6/03176-5

Korja, A. & Heikkinen, P., 2005. The accretionary Svecofennian orogen – insight from the BABEL profiles. Precambrian Research 136, 241–268. https://doi.org/10.1016/J.PRECAMRES.2004.10.007

Korsman, K., Holtta, P., Hautala, T. & Wasenius, P., 1984. Metamorphism as an indicator of evolution and structure of the crust in eastern Finland. Geological Survey of Finland, Bulletin 328, 40 p.

Korsman, K., Korja, T., Pajunen, M. & Virransalo, P., 1999. The GGT/SVEKA Transect: Structure and Evolution of the Continental Crust in the Paleoproterozoic Svecofennian Orogen in Finland. International Geology Review 41, 287–333. https://doi.org/10.1080/00206819909465144

Kukkonen, I. T. & Lauri, L. S., 2009. Modelling the thermal evolution of a collisional Precambrian orogen: High heat production migmatitic granites of southern Finland. Precambrian Research 168, 233–246. https://doi.org/10.1016/j.precamres.2008.10.004

Kurhila, M., Vaasjoki, M., Mänttäri, I., Rämö, T. & Nironen, M., 2005. U-Pb ages and Nd isotope characteristics of the Lateorogenic, migmatizing microcline granites in southwestern Finland. Bulletin of the Geological Society of Finland 77, 105–128. https://doi.org/10.17741/bgsf/77.2.002

Kurhila, M., Mänttäri, I., Vaasjoki, M., Rämö, O. T. & Nironen, M., 2011. U–Pb geochronological constraints of the late Svecofennian leucogranites of southern Finland. Precambrian Research 190, 1–24. https://doi.org/10.1016/j.precamres.2011.07.008

Lahtinen, R., 1996. Geochemistry of Palaeoproterozoic supracrustal and plutonic rocks in the Tampere-Hameenlinna area, southern Finland. Geological Survey of Finland, Bulletin 389, 113 p.

Lahtinen, R., Köykkä, J., Salminen, J., Sayab, M. & Johnston, S. T., 2023. Paleoproterozoic tectonics of Fennoscandia and the birth of Baltica. Earth-Science Reviews 246, 104586. https://doi.org/10.1016/j.earscirev.2023.104586

Lahti, S. & Kärkkäinen, N., 2009. Occurrence of REE minerals in the granites and granite-pegmatites of southern Finland. Geological Survey of Finland, Reports 28/2016, 28 p. (In Finnish)

Ludwig, K. R., 2003. User's manual for Isoplot/Ex, Version 3.00. A geochronological toolkit for Microsoft Excel. Berkeley Geochronology Center Special Publication 4, 72 p.

Mange, M. A. & Morton, A. C., 2007. Geochemistry of heavy minerals. In: Mange, M. A. & Wright, D. T. (eds.), Heavy

minerals in use. Developments in Sedimentology 58, pp. 345–391. https://doi.org/10.1016/S0070-4571(07)58013-1

Maniar, P. D. & Piccoli, P. M., 1989. Tectonic discrimination of granitoids. Geological Society of American Bulletin 101, 635–643. https://doi.org/10.1130/0016-7606(1989)101<0635:tdog>2.3.co;2

McDonough, W. F. & Sun, S., 1995. The composition of the Earth. Chemical Geology 120, 223–253. https://doi.org/10.1016/0009-2541(94)00140-4

Montel, J. M., Razafimahatratra, D., de Parseval, P., Poitrasson, F., Moine, B., Seydoux-Guillaume, A. M. & Gibert, F., 2018. The giant monazite crystals from Manangotry (Madagascar). Chemical Geology 484, 36–50. https://doi.org/10.1016/j.chemgeo.2017.10.034

Mouri, H., Väisänen, M., Huhma, H. & Korsman, K., 2005. Sm-Nd garnet and U-Pb monazite dating of high-grade metamorphism and crustal melting in the West Uusimaa area, southern Finland. GFF 127, 123–128. https://doi.org/10.1080/11035890501272123

Müller, W., M. Shelley, Miller, P. & Broude, S., 2009. Initial performance metrics of a new custom-designed ArF excimer LA-ICPMS system coupled to a two-volume laser-ablation cell. Journal of Analytical atomic Spectrometry 24, 209–214. https://doi.org/10.1039/b805995k

Müller, A., Simmons, W., Beurlen, H., Thomas, R., Ihlen, P. M., Wise, M., ... & Zagorsky, V., 2022. A proposed new mineralogical classification system for granitic pegmatites–Part I: History and the need for a new classification. The Canadian Mineralogist 60, 203–227. https://doi.org/10.3749/canmin.1700088

Nachit, H., Ibhi, A., Abia, E. H. & Ohoud, M. B., 2005. Discrimination between primary magmatic biotites, reequilibrated biotites and neoformed biotites. Comptes Rendus Géoscience 337, 1415–1420. https://doi.org/10.1016/j.crte.2005.09.002

Nironen, M., 1997. The Svecofennian orogen: a tectonic model. Precambrian Research 86, 21–44. https://doi.org/10.1016/S0301-9268(97)00039-9

Nironen, M., Elliott, B. A. & Rämö, O. T., 2000. 1.88–1.87 Ga post-kinematic intrusions of the Central Finland Granitoid Complex: a shift from C-type to A-type magmatism during lithospheric convergence. Lithos 53, 37–58. https://doi.org/10.1016/S0024-4937(00)00007-4

Nironen, M. & Kurhila, M., 2008. The Veikkola granite area in southern Finland: emplacement of a 1.83–1.82 Ga plutonic sequence in an extensional regime. Bulletin of the Geological Society of Finland 80, 39–68. https://doi.org/10.17741/bgsf/80.1.003

Nironen, M. (ed.), 2017. Bedrock of Finland at the Scale 1: 1 000 000: Major Stratigraphic Units, Metamorphism and Tectonic Evolution. Geological survey of Finland, Special Paper 60, 128 p.

Pajunen, M., Airo, M. L., Elminen, T., Mänttäri, I., Niemelä, R., Vaarma, M., ... & Wennerström, M., 2008. Tectonic evolution of the Svecofennian crust in southern Finland. In: Pajunen, M. (ed.), Tectonic evolution of the Svecofennian crust in southern Finland – a basis for characterizing bedrock technical properties. Geological Survey of Finland, Special Paper 47, pp. 15–160.

Peccerillo, A. & Taylor, S. R., 1976. Geochemistry of Eocene Calc-Alkaline Volcanic Rocks from the Kastamonu Area, Northern Turkey. Contributions to Mineralogy and Petrology 58, 63–81. https://doi.org/10.1007/BF00384745

Prior, D. J., 1993. Sub-critical fracture and associated retrogression of garnet during mylonitic deformation. Contributions to Mineralogy and Petrology 113, 545–556. https://doi.org/10.1007/BF00698322

Prior, D. J., Wheeler, J., Brenker, F. E., Harte, B. & Matthews, M., 2000. Crystal plasticity of natural garnet: New microstructural evidence. Geology 28, 1003–1006. https://doi.org/10.1130/0091-7613(2000)28<1003:CPONGN>2.0.CO;2

Prior, D. J., Wheeler, J., Peruzzo, L., Spiess, R. & Storey, C., 2002. Some garnet microstructures: an illustration of the potential of orientation maps and misorientation analysis in microstructural studies. Journal of Structural Geology 24, 999–1011. https://doi.org/10.1016/S0191-8141(01)00087-6

Rasilainen, K., Lahtinen, R. & Bornhorst, T. J., 2007. The Rock Geochemical Database of Finland Manual. Geological Survey of Finland, Report of Investigation 164, 38 p.

Räisänen, E., 1989. Uraniferous granitic veins in the Svecofennian schist belt in Nummi-Pusula, southern Finland. In: Uranium deposits in magmatic and metamorphic rocks. International Atomic Energy Agency (IAEA), Vienna, pp. 37–43.

Salminen, P. E., Hölttä, P., Lahtinen, R. & Sayab, M., 2022. Monazite record for the Paleoproterozoic Svecofennian orogeny, SE Finland: An over 150-Ma spread of monazite dates. Lithos 416, 106654. https://doi.org/10.1016/j.lithos.2022.106654

Sarapää, O., Lauri, L. S., Ahtola, T., Al Ani, T., Grönholm, S., Kärkkäinen, N., Lintinen, P., Torppa, A. & Turunen, P., 2015. Discovery Potential of Hi-Tech Metals and Critical Minerals in Finland. Geological Survey of Finland, Report of Investigation 219, 54 p.

Schreurs, J. & Westra. L., 1986. The thermotectonic evolution of a Proterozoic, low pressure, granulite dome, West Uusimaa, SW Finland. Contributions to Mineralogy and Petrology 93, 236–250. https://doi.org/10.1007/BF00371326

Schreyer, W., 1985. Experimental studies on cation substitutions and fluid incorporation in cordierite. Bulletin de Minéralogie 108, 273–291. https://doi.org/10.3406/bulmi.1985.7829

Seppänen, H., 1981. Selostus Kovelan monatsiittiaiheen tutkimuksista Nummi-Pusulan kunnassa 1980–1981. Geological Survey of Finland, Report M 19/2023/-81/1/60. (In Finnish)

Skyttä, P., Käpyaho, A. & Mänttäri, I., 2005. Supracrustal Rocks in the Kuovila Area, Southwestern Finland: Structural Evolution, Geochemical Characteristics and the Age of Volcanism. Bulletin of the Geological Society of Finland 77, 129–150. https://doi.org/10.17741/bgsf/77.2.003

Skyttä, P. & Mänttäri, I., 2008. Structural Setting of Late Svecofennian Granites and Pegmatites in Uusimaa Belt, SW Finland: Age Constraints and Implications for Crustal Evolution. Precambrian Research 164, 86–109. https://doi.org/10.1016/j.precamres.2008.04.001

Spear, F. S., 1993. Metamorphic phase equilibria and pressure–temperature–time paths. Mineralogical Society of America Monograph, 799 p.

Streckeisen, A., 1976. To each plutonic rock its proper name. Earth-science reviews 12, 1–33. https://doi.org/10.1016/0012-8252(76)90052-0

Streckeisen, A. & Le Maitre, R. W.,1979. A chemical approximation to the modal QAPF classification of the igneous rocks. New Yearbook of Mineralogy, Papers 136, 169–206.

Suominen, V., 1991. The Chronostratigraphy of Southwestern Finland with Special Reference to Postjotnian and Subjotnian Diabases. Geological Survey of Finland, Bulletin 356, 100 p.

Thomas, R. & Davidson, P., 2008. Water and melt/melt immiscibility, the essential components in the formation of pegmatites; evidence from melt inclusion. Geologische Wissenschaften 36, 347–364.

Thomas, R. & Davidson, P., 2012a. Water in granite and pegmatite-forming melts. Ore Geology Reviews 46, 32–46. http://doi.org/10.1016/j.oregeorev.2012.02.006

Thomas, R. & Davidson, P. 2012b. Evidence of a water-rich silica gel state during the formation of a simple pegmatite. Mineralogical Magazine 76, 2785–2801. http://doi.org/10.1180/minmag.2012.076.7.11

Thomas, R. & Davidson, P., 2013. The missing link between granites and granitic pegmatites. Journal of geosciences 58, 183–200. http://doi.org/10.3190/jgeosci.135

Thomas, R. & Davidson, P., 2014. Liquid immiscibility—important processes during pegmatite formation. In: Pan-American Current Research on Fluid Inclusions (PACROFI-Xll), U.S. Geological Survey and Colorado State University, Abstract Volume, pp. 52–53.

Thomas, R. & Davidson, P., 2016. Revisiting complete miscibility between silicate melts and hydrous fluids, and the extreme enrichment of some elements in the supercritical state—Consequences for the formation of pegmatites and ore deposits. Ore Geology Reviews 72, 1088–1101. http://doi.org/10.1016/j.oregeorev.2015.10.004

Torvela, T. & Kurhila, M., 2022. Timing of syn-orogenic, high-grade transtensional shear zone formation in the West Uusimaa Complex, Finland. Bulletin of the Geological

Society of Finland 94, 5–22. https://doi.org/10.17741/bgsf/94.1.001

Tuccillo, M. E, Essene, E. J. & van der Pluijm, B. A, 1990. Growth and retrograde zoning in garnets from high-grade, metapelites: Implications for pressure-temperature paths, Geology 18, 839–842. https://doi.org/10.1130/0091-7613(1990)018<0839:GARZIG>2.3.CO;2

Tröger, W. E., Bambauer, H. U., Taborszky, F. & Trochim, H. D., 1979. Optical determination of rock- forming minerals: part 1, determinative tables. Schweizerbart, Stuttgart, 188 p.

Van Lichtervelde, M., Goncalves, P., Eglinger, A., Colin, A., Montel, J. M. & Dacheux, N., 2021. Solubility of monazite–cheralite and xenotime in granitic melts, and experimental evidence of liquid–liquid immiscibility in concentrating REE. Journal of Petrology 62, egab020. https://doi.org/10.1093/petrology/egab020

Vasyukova, O. & Williams-Jones, A. E., 2014. Fluoride–silicate melt immiscibility and its role in REE ore formation: Evidence from the Strange Lake rare metal deposit, Québec-Labrador, Canada. Geochimica et Cosmochimica Acta 139, 110–130. https://doi.org/10.1016/j.gca.2014.04.031

Vasyukova, O. & Williams-Jones, A. E., 2016. The evolution of immiscible silicate and fluoride melts: Implications for REE ore-genesis. Geochimica et Cosmochimica Acta 172, 205–224. https://doi.org/10.1016/j.gca.2015.09.018

Veksler, I. V., Dorfman, A. M., Kamenetsky, M., Dulski, P. & Dingwell, D. B., 2005. Partitioning of lanthanides and Y between immiscible silicate and fluoride melts, fluorite and cryolite and the origin of the lanthanide tetrad effect in igneous rocks. Geochimica et Cosmochimica Acta 69, 2847–2860. https://doi.org/10.1016/j.gca.2004.08.007

Väisänen, M., Mänttäri, I. & Hölttä, P., 2002. Svecofennian Magmatic and Metamorphic Evolution in Southwestern Finland as Revealed by U-Pb Zircon SIMS Geochronology. Precambrian Research 116, 111–127. https://doi.org/10.1016/S0301-9268(02)00019-0

Väisänen, M. & Kirkland, C. L., 2008. U-Th-Pb zircon geochronology on igneous rocks in the Toija and Salittu Formations, Orijärvi area, southwestern Finland: constraints on the age of volcanism and metamorphism. Bulletin of the Geological Society of Finland 80, 73–87. https://doi.org/10.17741/bgsf/80.2.001

Wu, C. M., Zhang, J. & Ren, L. D., 2004. Empirical Garnet-Biotite-Plagioclase-Quartz (GBPQ) Geobarometry in Medium- to High-Grade Metapelites. Journal of Petrology 45, 1907–1921. https://doi.org/10.1093/petrology/egh038

Zheng, Y. F. & Gao, P., 2021. The production of granitic magmas through crustal anatexis at convergent plate boundaries. Lithos 402, 106232. https://doi.org/10.1016/j.lithos.2021.106232